The beneficial effect of cyclohexyl substituent on the in vitro anticancer activity of diiron vinyliminium complexes

The Beneficial Effect of Cyclohexyl Substituent on the In Vitro Anticancer Activity of Diiron Vinyliminium Complexes

Sara Benetti,[a,$] Maria Dalla Pozza,[b,$] Lorenzo Biancalana,[a] Stefano Zacchini,[c] Gilles Gasser,[b,*] Fabio Marchetti [a,*]

[a] University of Pisa, Dipartimento di Chimica e Chimica Industriale, 56124 Pisa, Italy.

[b] Chimie ParisTech, PSL University, CNRS, Institute of Chemistry for Life and Health, Paris, France.

[c] University of Bologna, Dipartimento di Chimica Industriale "Toso Montanari", 40136 Bologna, Italy.

Corresponding Authors

*E-mail addresses: gilles.gasser@chimieparistech.psl.eu; fabio.marchetti@unipi.it

Webpages: http://www.gassergroup.com/; https://people.unipi.it/fabio_marchetti/

[$] these authors have contributed equally to the work.

ORCID-ID:

Sara Benetti: 0000-0003-3465-8559

Maria Dalla Pozza: 0000-0002-6331-2920

Lorenzo Biancalana: 0000-0002-9276-0095

Stefano Zacchini: 0000-0003-0739-0518

Gilles Gasser: 0000-0002-4244-5097

Fabio Marchetti: 0000-0002-3683-8708

Abstract

Novel diiron vinyliminium complexes, $[Fe_2Cp_2(CO)(\mu\text{-}CO)\{\mu\text{-}\eta^1\text{:}\eta^3\text{-}C(R^3)\text{=}CHC\text{=}NMe(R^2)\}]CF_3SO_3$ (**2a-f**; R^2 = 4-C_6H_4OMe, Cy or Me; R^3 = Cy, CH_2Cy or 4-C_6H_4OMe; Cy = cyclohexyl, Cp = η^5-C_5H_5), were synthesized by alkyne insertion reaction from the corresponding diiron aminocarbyne precursors, and isolated in 53-98% yields. The reactions of selected vinyliminium complexes with N_2CHCO_2Et and MeONa, followed by *N*-methylation, afforded the new hydrazone-vinyliminium $[Fe_2Cp_2(CO)(\mu\text{-}CO)\{\mu\text{-}\eta^1\text{:}\eta^3\text{-}C(R^3)C(NMeN\text{=}CHCO_2Et)CN(R^1)(R^2)\}]X$ (**4a-c**; R^1 = Me or CH_2Ph; R^2 = Cy, CH_2Ph or Me; R^3 = 4-C_6H_4OMe or Ph; X = NO_3 or CF_3SO_3), in 53-67% yields. Compounds **2a-f** and **4a-c** were fully characterized by IR and multinuclear NMR spectroscopy, and the structures of **2a-c** were ascertained by single crystal X-ray diffraction. Moreover, D_2O solubility, Log P_{ow} coefficients and the fraction of each complex preserved in aqueous media after 72 hours at 37 °C were determined by ^{1}H NMR and UV-Vis methods. The antiproliferative activity of **2a-f** and **4a-c** was measured on the mouse colon CT26 and human glioblastoma U87 cancer cell lines, and on the retinal pigment epithelial RPE-1 non-cancerous cell line. Complexes **2a,d,e**, which all bear R^3 = Cy, stand out for their performance and their selectivity towards cancer cells. To give insight into the mechanism of action, the effect of **2a**, **2d**, **2e**, **2f**, **4b** and **4c** on the mitochondrial respiration was evaluated in CT26 cells (Seahorse Mito Stress Test), revealing a correlation between the effectiveness of the complexes and their influence on the mitochondrial metabolism.

Keywords: diiron complexes; alkyne insertion; anticancer; bioorganometallic chemistry; metals in medicine.

Introduction

Transition metal complexes can play an important role in the development of new and efficient anticancer drugs, due to their peculiar properties including a wide availability of structures and geometries, a feasible redox chemistry centred on the metal, and the possible incorporation (and dissociation) of a variety of bioactive fragments.[1,2,3,4] Nowadays, a few platinum compounds are used worldwide in the hospital treatment of different types of tumours[5,6,7] but, despite their efficacy, they manifest some limitations arising from severe side effects and resistance phenomena.[8,9,10] To overcome these limitations, compounds based on other transition metals have been widely considered as alternatives,[11,12,13,14] and, in this regard, endogenous metals may represent a convenient choice to substantially reduce toxicity issues.[15,16] Concerning iron complexes, organometallic iron(II) compounds based on the ferrocene skeleton have emerged as a promising category (Figure 1).[17,18,19,20] Several of them have been investigated *in vivo* showing significant tumour inhibition and low acute toxicity,[21,22,23,24] while ferrocifens exert a potent antiproliferative activity *in vitro* associated with the production of reactive oxygen species (ROS) promoted by Fe^{II} to Fe^{III} intracellular oxidation.[25,26] This research has been extended to half-sandwich iron(II) cyclopentadienyl complexes[18,27] and, recently, we have unveiled the anticancer potential of diiron(I) complexes based on the $\{Fe_2Cp_2(CO)_x\}$ core (x = 2-3, Cp = η^5-C_5H_5).[28] Basically, this dimetallic core enables cooperative effects resulting in greater synthetic opportunities,[29,30,31,32] and, for instance, cationic aminocarbyne and vinyliminium species (Figure 1, structures ***IV*** and ***V***) can be easily obtained, even in multigram scales, exploiting straightforward synthetic routes.[33,34,35] Complexes ***IV*** and ***V*** are generally robust in physiological solutions, and their cytotoxicity is mainly related to the intracellular disaggregation of the diiron structure, leading to iron(I) species being responsible for enhanced ROS (reactive oxygen species) production and inhibition of TrxR (thioredoxin reductase).[36,37,38,39] Complexes ***V*** display a range of physico-chemical behaviours and antiproliferative activities, depending on the combination of substituents ($R^{1\text{-}3}$).[37,40,41] The vinyliminium moiety in ***V*** is generated through the incorporation of a terminal alkyne ($HC{\equiv}CR^3$) according to a general reaction, which is tolerant of a variety of functional groups within R^3, therefore complexes ***V*** constitute a potentially unlimited class of organometallics. Structural-activity relationship studies

highlighted a substantial beneficial effect to the cytotoxicity of the diiron complexes, and to their selectivity towards cancer cells, of 4-C_6H_4OMe, cyclohexyl (Cy) and benzyl as R^2 substituents in combination with R^1 = Me. The favourable role of the 4-methoxyphenyl group was previously observed on both organic[42] and inorganic drugs, while the Cy moiety has been regarded to facilitate the cellular drug uptake due to its compact and hydrophobic structure.[43,44,45] Furthermore, a statistical analysis on the bioactivity of almost 50 type ***V*** compounds indicates the opportunity to introduce alkyl groups as R^3-substituents to increase cancer cell selectivity.[46]

In the present work, we report on the synthesis, the characterization, and a study of the anticancer potential of six new diiron vinyliminium complexes containing the above-mentioned substituents, including combinations of both 4-C_6H_4OMe and Cy within the same compound. As a further exploration of the structure-activity relationship, three new vinyliminium complexes decorated with a hydrazone fragment, $\{(CO_2Et)CH=N-N(Me)-C\}$, have been prepared and evaluated. We note that the hydrazone motif has been widely investigated for biological applications,[47,48,49] especially hydrazones possessing an azomethine hydrogen, $\{CH=N-N\}$, which represent an important class of compounds for new drug development.[50] In addition, some metal complexes containing hydrazone ligands have revealed a promising antiproliferative activity.[51,52,53]

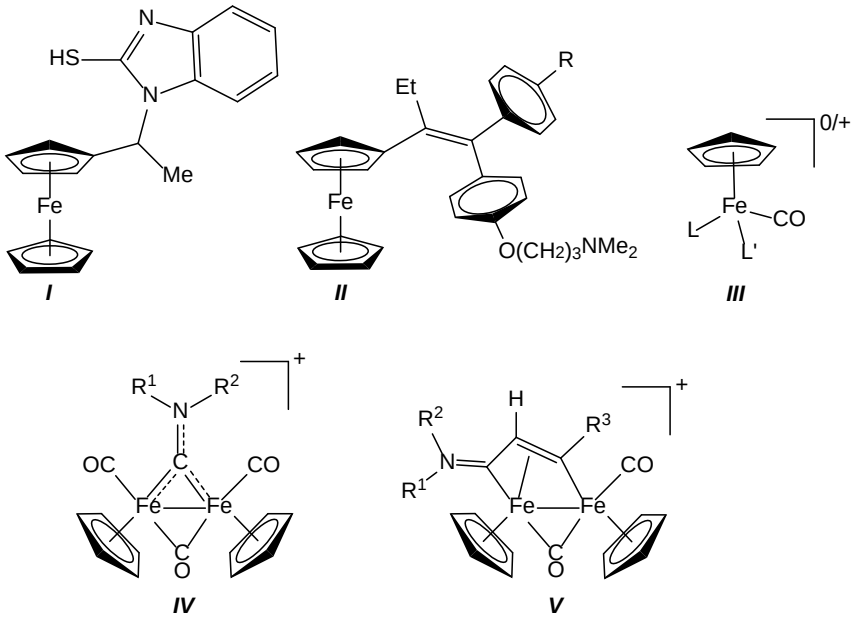

I ***II*** ***III***

IV ***V***

Figure 1. Mono- and diiron cyclopentadienyl compounds with documented anticancer activity: ***I***) ferrocene derivative investigated *in vivo* on murine carcinoma 755; ***II***) ferrocifens (R = H, OH); ***III***) half-sandwich iron complexes (L, L' = halide, pseudohalide, carbonyl, (di)phosphine, nitrile, imidazole);[18,27] ***IV***) diiron μ-aminocarbyne complexes (R^1, R^2 = alkyl or aryl; triflate salts); ***V***) diiron μ-vinyliminium complexes (R^1, R^2 = alkyl or aryl; R^3 = alkyl, aryl, $SiMe_3$, carboxylate, thiophenyl, pyridine, ferrocenyl; triflate salts).[37,40,41]

Results and discussion

1. Synthesis and characterization of diiron complexes

The μ-aminocarbyne complexes $[Fe_2Cp_2(CO)_2(\mu\text{-}CO)\{\mu\text{-}CNMe(R)\}]CF_3SO_3$, **1a-d**, readily available from multigram scale synthesis, were first converted into the mono-acetonitrile adducts $[Fe_2Cp_2(CO)(NCMe)(\mu\text{-}CO)\{\mu\text{-}CNMe(R)\}]CF_3SO_3$ (R = Me, 4-C_6H_4OMe, Cy, CH_2Ph)[54] using the TMNO (trimethylamine-N-oxide) strategy.[55,56,57] The acetonitrile complexes, in dichloromethane solution, were then treated with a slight molar excess of a range of terminal alkynes containing cyclohexyl and/or *para*-methoxyphenyl substituents. Removal of the labile acetonitrile ligand by the alkyne is followed by regioselective alkyne insertion into the iron-bridging carbyne, to afford the vinyliminium products **2a-f** (Scheme 2).

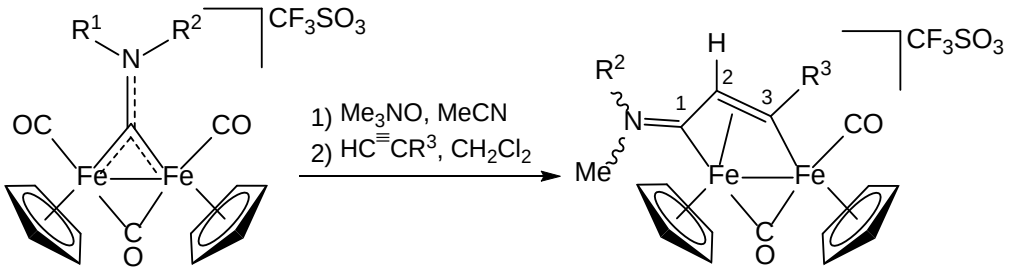

	R^2	R^3	
1a	4-C_6H_4OMe	Cy	**2a**
1a	4-C_6H_4OMe	CH_2Cy	**2b**
1b	Cy	4-C_6H_4OMe	**2c**
1b	Cy	Cy	**2d**
1c	CH_2Ph	Cy	**2e**
1d	Me	4-C_6H_4OMe	**2f**

Scheme 1. Two-step synthesis of diiron vinyliminium complexes via coupling of bridging aminocarbyne ligands with terminal alkynes (R^1 = Me).

Products **2a-f** were isolated in 53-98% yields after alumina chromatography, and fully characterized by elemental analysis, IR and multinuclear NMR spectroscopy. The IR spectra (CH_2Cl_2 solutions) display a typical pattern with two bands due to terminal (1989-1991 cm^{-1}) and bridging carbonyl ligands (1803-1810 cm^{-1}), and another band ascribable to the iminium moiety and sensitive to R^2 (1640-1680 cm^{-1}).

The NMR spectra of **2a-e** (acetone-d_6 solutions, Figures S1-S10) contain two sets of resonances, due to *E-Z* isomerism arising from the different substituents on the iminium nitrogen, with prevalence of the E form (the *E/Z* ratio ranging from 1 in **2d** to 3 in **2b**). Instead, **2f** exists as a single isomeric species (Figures S11-S12). As previously documented for several analogous diiron vinyliminium complexes, *E* and *Z* isomers are usually not interconvertible or separable.[34,58] In general, *E* and *Z* isomers are distinguishable based on the resonance of the iminium methyl group: in the *Z* form compared to the E form, such signal is upfield shifted in the ^1H spectrum and downfield shifted in the ^{13}C spectrum. For instance, the methyl group in **2c** resonates at 3.98 (^1H) and 38.9 ppm (^{13}C) in the *E* isomer, and at 3.31 (^1H) and 44.1 ppm (^{13}C) in the *Z* isomer. In **2a-f**, the ^1H NMR resonances for the Cp ligands fall within the interval 5.00 - 5.78 ppm, indicating a mutual cis-geometry with respect to the Fe-Fe axis.[33,40,59] The most significant ^{13}C NMR features are given by the resonances related to the vinyliminium carbon chain, falling respectively in the ranges 224.9-231.1 ppm (C^1), 46.0-54.3 ppm (C^2) and 204.8-221.1 ppm (C^3). The characteristic low-field resonances evidence the amino-alkylidene character of C^1 and the bridging alkylidene character of C^3.[31,60,61,62,63]

Crystals of **2a**, **2b** and **2c** suitable for X-ray diffraction analysis were collected by slow diffusion of diethyl ether into dichloromethane solutions of the compounds. The structures exhibit *cis* arrangement of the Cp ligands, in agreement with the NMR data. The iminium group displays *E* geometry in **2a** and **2b**, while the *Z* configuration has been recognized for **2c**; accordingly, the *E* isomer of **2a-b** is prevalent over the *Z* one in solution (*E/Z* ratio ≈ 3), while *E* and *Z* isomers are in almost equimolar amounts in **2c**. In general, bonding parameters and geometries of **2a-c** closely resemble to previously reported analogous diiron vinyliminium complexes (Figure 2, Table 1). Thus, C(3)-C(4) and C(4)-C(5)

bond lengths are similar [*e.g.* 1.414(4) and 1.423(4) Å, respectively, in **2a**], suggesting extensive charge delocalization along the vinyliminium chain. The C(3)-N(1) distance [*e.g.* 1.296(4) Å in **2a**] is indicative of substantial double bond character, in alignment with the observation of *E* and *Z* isomers in solution.

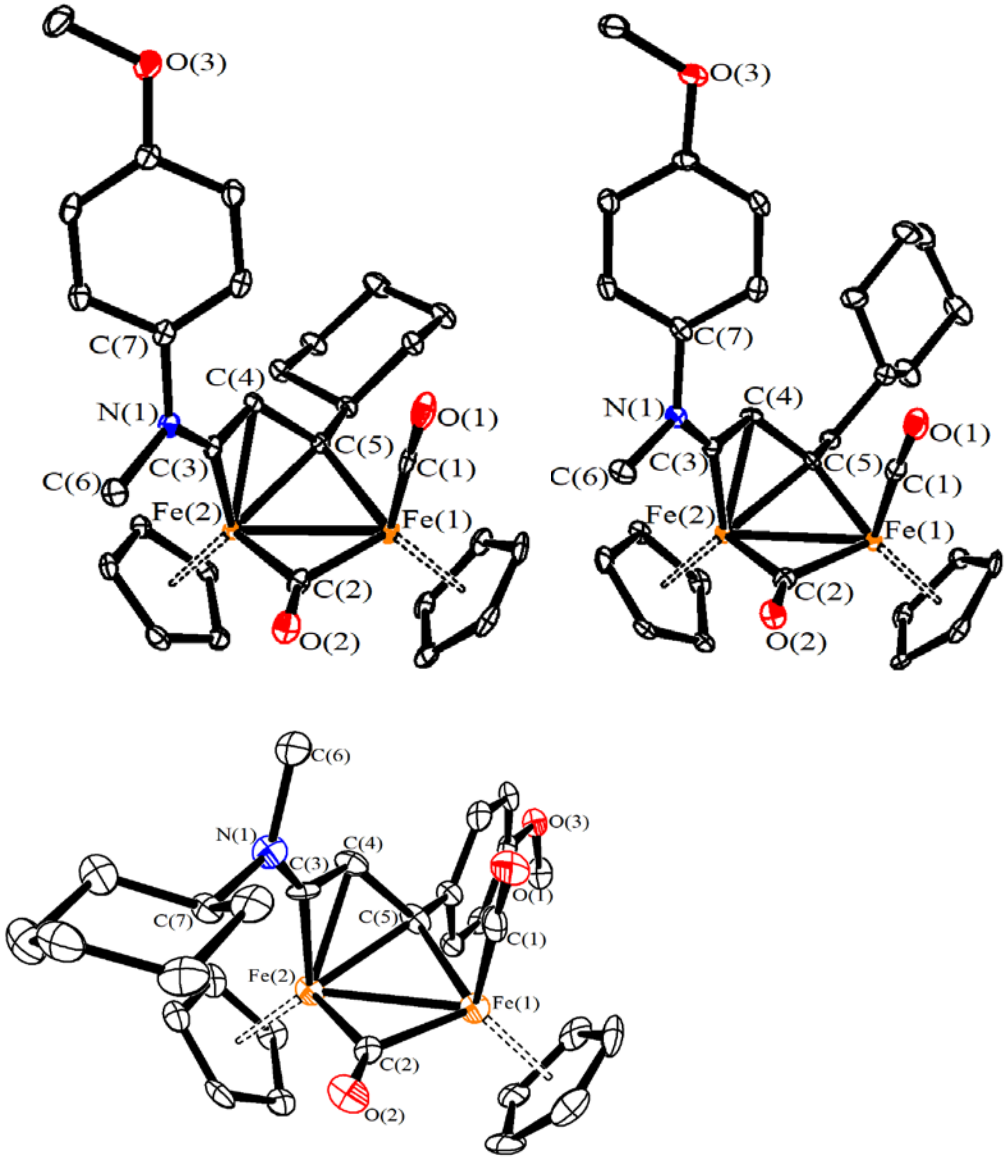

Figure 2. View of the structures of the cations of **2a**, **2b** and **2c**, with key atoms labelled. Displacement ellipsoids are at the 30% probability level. Hydrogen atoms have been omitted for clarity.

Table 1. Selected bond lengths (Å) and angles (°) for **2a**, **2b** and **2c**.

	2a	**2b**	**2c**
Fe(1)-Fe(2)	2.5395(6)	2.5266(11)	2.558(3)

Fe(1)-C(1)	1.749(3)	1.750(6)	1.795(15)
Fe(1)-C(2)	1.911(3)	1.919(6)	1.919(12)
Fe(2)-C(2)	1.944(3)	1.929(6)	1.949(13)
Fe(2)-C(3)	1.840(3)	1.843(6)	1.864(11)
Fe(2)-C(4)	2.065(3)	2.050(5)	2.042(13)
Fe(2)-C(5)	2.032(3)	2.030(5)	2.035(12)
Fe(1)-C(5)	1.983(3)	1.962(6)	1.966(15)
C(1)-O(1)	1.146(4)	1.138(7)	1.111(15)
C(2)-O(2)	1.164(4)	1.161(7)	1.144(14)
C(3)-N(1)	1.296(4)	1.295(7)	1.265(15)
C(3)-C(4)	1.414(4)	1.401(8)	1.402(17)
C(4)-C(5)	1.423(4)	1.430(8)	1.408(18)
Fe(1)-C(1)-O(1)	177.6(3)	176.1(5)	178.5(13)
Fe(1)-C(2)-Fe(2)	82.41(12)	82.1(2)	82.8(5)
Fe(1)-C(5)-Fe(2)	78.45(10)	78.52(19)	79.5(5)
C(3)-N(1)-C(6)	119.6(3)	119.3(5)	120.6(11)
C(3)-N(1)-C(7)	123.5(2)	123.8(5)	121.0(11)
C(6)-N(1)-C(7)	116.8(2)	116.9(4)	118.2(9)
C(3)-C(4)-C(5)	117.1(3)	117.8(5)	117.5(12)

The vinyliminium ligand in complexes like **2a-c** usually manifests Brønsted acidity, and the deprotonation of the C^2-H leads to an elusive carbene intermediate, which can be captured by suitable organic fragments to afford stable derivatives with a functionalized bridging hydrocarbyl ligand. By exploiting this strategy and on account of the biological properties of the hydrazone function (see Introduction), a series of diiron vinyliminium complexes were allowed to react with sodium methoxide in the presence of ethyl diazoacetate (Scheme 2). Thus, the reactions of the newly prepared **2c** and the already known **2g** and **2h** led to the azine complexes **3a-c**. The latter are analogous to compounds previously reported and characterized, showing *cis* geometry of the Cp ligands.[64] Compounds **3a-c** are air-sensitive and especially **3a-b** underwent a slow decomposition at room temperature even when maintained under N_2 atmosphere, preventing their NMR characterization. The IR spectrum pattern of **3a-c** (in dichloromethane) is fully consistent with data available for analogous complexes, with two bands related to the carbonyl ligands (e.g. at 1960 and 1775 cm^{-1} in the case of **3c**), and additional absorptions due to the ester function and the C=N double bond within the azine moiety (1711 and 1589 cm^{-1}, respectively, for **3c**). The ^{1}H NMR spectrum of **3c** (in CD_2Cl_2, Figure S19) contains two sets of resonances, which

have been attributed to stereoisomers arising from the different orientations of the azine substituents H and CO_2Et (E-Z isomers). Consistent with this hypothesis, the Cp signals are close for the two isomers (4.88 and 4.52 ppm; 4.73 and 4.66 ppm), while one methyl group resonates at significantly different chemical shifts in the two isomers (i.e., 3.08 and 2.60 ppm).

The hydrazone-vinyliminium complexes **4a-b** were synthesized in good yields as nitrate salts via a two-step reaction, consisting in the treatment of **3a-b** with an excess of methyl iodide, followed by metathesis with $AgNO_3$. On the other hand, **4c** was obtained as triflate salt in 62% yield, by direct addition of methyl triflate to **3c**.

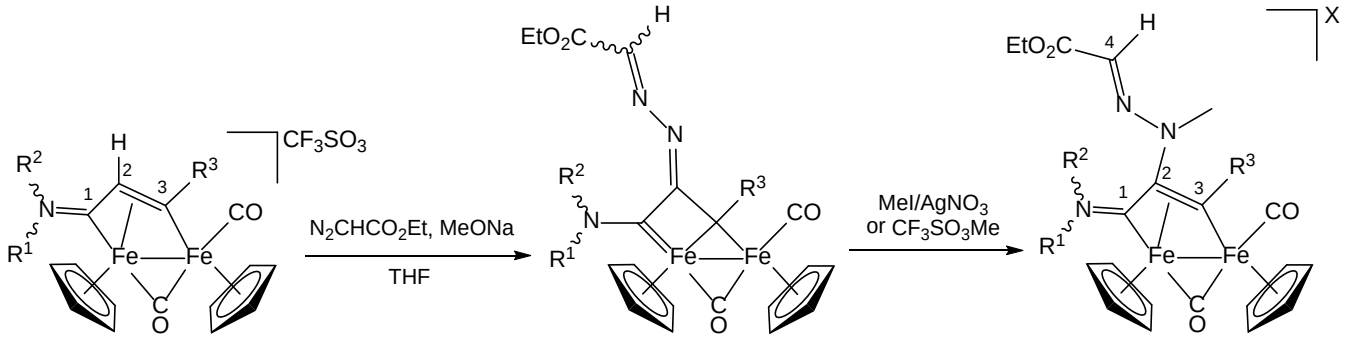

	R^1	R^2	R^3		X	
2c	Me	Cy	4-C_6H_4OMe	**3a**	NO_3	**4a**
2g	CH_2Ph	CH_2Ph	Ph	**3b**	NO_3	**4b**
2h	Me	Me	Ph	**3c**	CF_3SO_3	**4c**

Scheme 2. Coupling of ethyl diazoacetate with deprotonated vinyliminium ligand, and subsequent methylation of the azine function leading to hydrazone-vinyliminium complexes.

The IR spectra of **4a-c** (in CH_2Cl_2) display the typical pattern of cationic diiron vinyliminium complexes, with three bands related to the terminal and bridging carbonyl ligands and the iminium (C^1=N) moiety (e.g., at 1995, 1815 and 1667 cm^{-1} in the case of **4c**). In addition, the hydrazone moiety manifests itself with the absorptions related to the C^4=N and CO_2Et groups (1709 and 1568 cm^{-1} for **4c**).

The NMR spectra of **4a** (Figures S13-S14) consist of two sets of resonances, attributed to *E* and *Z* isomers with the latter slightly prevalent, indicating that a partial inversion of configuration takes place ongoing from **2c** to **4a**, as expected due to the introduction of the bulky hydrazone moiety on the C^2 carbon. Regarding **4a**, the diagnostic signals for the methyl group bound to C^1N occur at 3.94 (^1H) and 38.0 ppm (^{13}C) in the *E* isomer, and at 3.01 (^1H) and 42.3 ppm (^{13}C) in the Z isomer. Based on NMR spectroscopy, both **4b** and **4c**, comprising identical C^1N substituents, exist in solution essentially as a single isomeric form (Figures S15-S18). In analogous hydrazone-vinyliminium complexes, the *E* arrangement of the C^4-substituents (i.e., with the ester group pointing far away from the terminal carbonyl ligand) is largely favourable over the *Z* one, and it is reasonable that the same geometry is present in **4a-c**. Minor signals accounting for a secondary isomeric form have been detected in the ^1H spectrum of **4c**, and might be attributable to a very low amount of trans (Cp) or Z (hydrazone) isomer.

In the ^1H NMR spectra of **4a-c**, the hydrazone moiety gives rise to a relatively low field signal due to the iminium hydrogen (e.g., at 6.41 ppm for **4b**), while the singlet of the methyl introduced with the methylation reaction occurs at ca. 2.7 ppm.

Salient ^{13}C NMR features of **4a-c** are the resonances detected in the intervals 222.9 - 228.7 ppm (C^1), 83.8 – 90.7 ppm (C^2) and 191.2 – 204.5 ppm (C^3), which are indicative of the vinyliminium nature of the $N=C^1–C^2=C^3$ chain. The C^4 carbon was found to resonate at 121.3 – 123.1 ppm, coherently with its alkenic nature.

2. Solubility and stability in aqueous media, and octanol-water partition coefficients.

In view of the biological studies, the behaviour in aqueous media of the new complexes **2a-f** and **4a-c** was investigated by spectroscopic techniques (see Table 2 and Experimental for details). First, the solubility of the complexes was measured in D_2O by means of ^1H NMR spectroscopy using dimethylsulfone ($DMSO_2$) as internal standard. All complexes resulted sufficiently soluble[65] [solubility values range from 0.40 mM (**2b**) to 4.8 mM (**4a**); cisplatin:[66] 8.4 mM]. The solubility of **2a** and **2d** was

further assessed by ICP-OES and UV-Vis methods, showing an approximate agreement between the three employed techniques (Table S1).

The octanol-water partition coefficients were obtained by UV-Vis method. In general, compounds display an amphiphilic character, with Log P_{ow} values variable from -0.31 (**2f**) to 0.83 (**2d**). Complex **4b** is out of this range (> 1.5), and its substantial lipophilicity appears correlated with the presence of three phenyl rings. On the other hand, **4a** displays the highest D_2O solubility ($4.8 \cdot 10^{-3}$ M) associated with a balanced hydrophilic/lipophilic character (Log P_{ow} = 0.07), see Figure 3A.

To increase the solubility of the complexes and considering that dimethylsulfoxide (DMSO) was used to help their dissolution during the cytotoxicity tests (*vide infra*), ^{1}H NMR stability studies were conducted on deuterated dimethylsulfoxide-water mixtures stored at 37 °C ($DMSO_2$ as internal standard, see Table S2 and Figures S20-S28; **4a** was studied in pure D_2O). In general, **2a-f** and **4a-c** display a notable inertness, with 63-95% of the starting material detected after 3 days (Figure 3B).

The behaviour of the complexes was then assessed in a deuterated cell culture medium (DMEM-d) in admixture with DMSO-d_6 (except **4a**), at 37 °C (Figures S29-S37). Interestingly, **2a-f** maintained a substantial robustness (74-93% of the starting material detected after 3 days, see Figure 3B). On the other hand, the hydrazone-vinyliminium species showed a significant drop in their stability. The degradation of these compounds increases along the series **4a** < **4b** < **4c** and is accelerated in the cell culture medium; it is presumable that it involves the hydrolysis of the hydrazone fragment,[67] being favoured by the positive charge on the adjacent vinyliminium moiety. According to Dynamic Light Scattering experiments on phosphate buffer solutions with 10% foetal bovine serum (FBS), selected diiron complexes may form nanoaggregates[68] (Table S3), which might be related to the disassembly of the diiron structure which is related to the cytotoxicity, as it has been previously observed on analogous diiron bis-cyclopentadienyl complexes.[28,36]

Table 2. Solubility in D_2O (based on ^1H NMR spectroscopy, $DMSO_2$ as internal standard) and partition coefficients (Log P_{ow}) of diiron complexes (T = 21 °C). Residual % of complex in aqueous media after 72 hours at 37 °C, and solvent (D_2O or DMEM-d) over DMSO-d_6 ratio.

Complex	Solubility / mol·L^{-1}	Log P_{ow}	% D_2O/DMSO-d_6	% DMEM-d/DMSO-d_6	Solvent/DMSO-d_6 ratio
2a	$4.8 \cdot 10^{-4}$	0.56 ± 0.03	83	83	4
2b	$4.0 \cdot 10^{-4}$	0.80 ± 0.02	89	74	4
2c	$7.3 \cdot 10^{-4}$	0.49 ± 0.03	81	93	3
2d	$5.7 \cdot 10^{-4}$	0.83 ± 0.03	84	89	4
2e	$6.4 \cdot 10^{-4}$	0.65 ± 0.01	92	87	3
2f	$3.7 \cdot 10^{-3}$	–0.31 ± 0.04	53	65	∞
4a	$4.8 \cdot 10^{-3}$	0.07 ± 0.08	88	64	∞
4b	$4.0 \cdot 10^{-4}$	> 1.5	95	42	4
4c	$9.3 \cdot 10^{-4}$	–0.07 ± 0.02	72	0	6

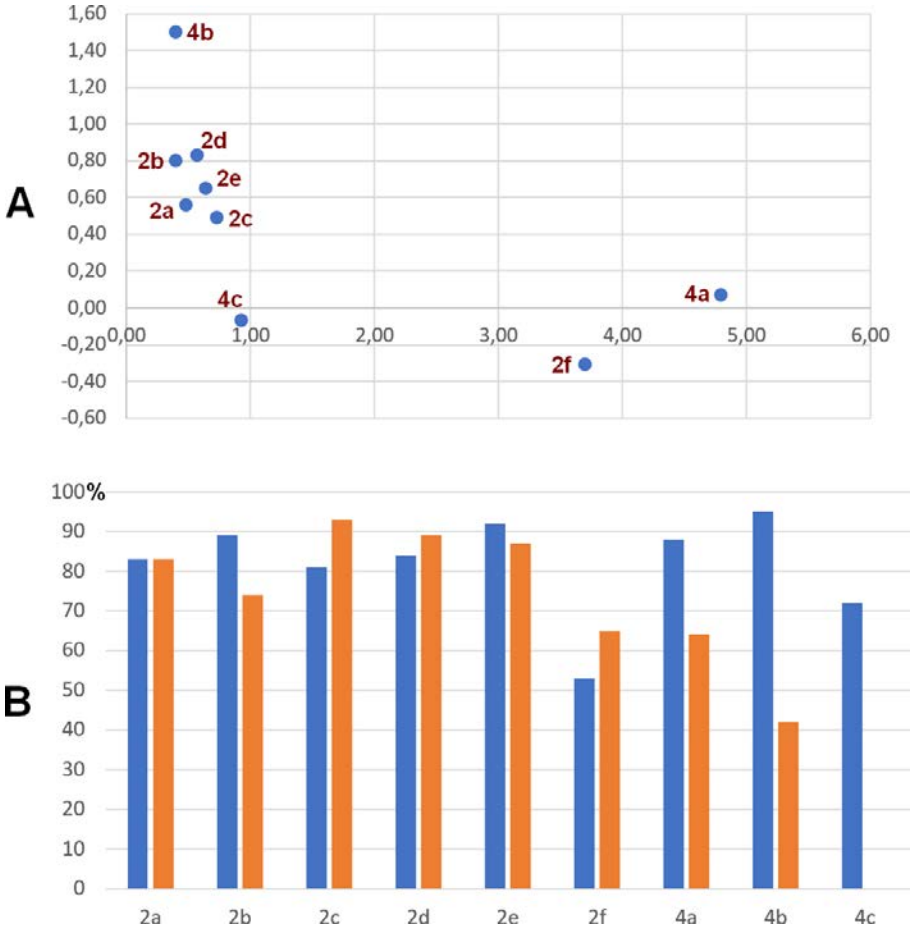

Figure 3. A) Log P_{ow} (vertical axis) vs. solubility ($\cdot 10^{-3}$ M in D_2O, ^1H NMR; horizonal axis) of diiron complexes. B) Residual % of complexes in aqueous media after 72 hours at 37 °C (blue: D_2O/DMSO-d_6 solution; orange: DMEM-d/DMSO-d_6 solution).

3. Cytotoxicity studies

The cytotoxic activity of the complexes was to check the possible cytotoxic selectivity against cancer cells. Cisplatin was used as reference drug, and the diiron aminocarbyne precursors **1b** and **1c** were also analysed. The obtained IC_{50} values are compiled in Table 3. In general, the investigated vinyliminium complexes display a considerable cytotoxicity on the two cancer cell lines, with IC_{50} values falling in the low micromolar range. The activity of the most performant compounds, i.e., **2a,b,d,e** and **4d**, is comparable to that of cisplatin. The exception is represented by **4c**, for which a moderate activity was recognized, probably correlated with the instability of this complex in the cell culture medium (see above).

Remarkably, the vinyliminium complexes **2a-f** manifest an interesting selectivity of action. As a matter of fact, the selectivity index (S.I)., defined as the ratio between the IC_{50} values in human noncancerous cells (RPE-1) and human cancer cells (U87) respectively, approximately matches that of cisplatin in the case of **2c**, but it is higher in the other cases, and 3-5 fold higher in **2a,d,e**, containing a cyclohexyl group on C^3.

Overall, collected data indicate that the presence of a cyclohexyl group on the vinyl C^3 carbon produces a strongly beneficial effect on the *in vitro* anticancer efficacy and improves the selectivity of related diiron vinyliminium complexes against cancer cells. The introduction of a methylene linker between the cyclohexyl and C^3 determines a lower selectivity (compare **2a** with **2b**), and the exchange of position of 4-C_6H_4OMe and Cy groups is also detrimental (compare **2a** with **2c**). The "cyclohexyl effect" is evident when comparing the IC_{50} values of **2a,d,e** with data available in the literature for analogous diiron vinyliminium complexes, including sugar-derivatized vinyliminium complexes, related to the same cell lines and experimental conditions;[69] Table 3 shows data for the most performing compounds of such series (**2i,j**). Furthermore, the aminocarbyne complexes **1b** and **1c** are inactive against the CT26 cancer cell line, while a moderate activity was recognized on the non-cancer RPE-1 cell line. This outcome indicates the superior performance provided by the modification of the bridging aminocarbyne (C_1) ligand on diiron complexes into a vinyliminium (C_3), at least concerning the investigated cell lines.

Table 3. IC_{50} values (μM) determined for diiron complexes and cisplatin on CT26, U87 and RPE-1 cell lines after 48 h of treatment. Values are given as the mean ± SD. S.I. = selectivity index. **2i** = $[Fe_2Cp_2(CO)(\mu\text{-}CO)\{\mu\text{-}\eta^1\text{:}\eta^3\text{-}C^3(Ph)C^2HC^1NMe(2,6\text{-}C_6H_3Me_2)\}]CF_3SO_3$ and **2j** = $[Fe_2Cp_2(CO)(\mu\text{-}CO)\{\mu\text{-}\eta^1\text{:}\eta^3\text{-}C^3(Me)C^2(Me)C^1NMe(2,6\text{-}C_6H_3Me_2)\}]CF_3SO_3$ (literature data). The IC_{50} values were obtained from the average of three independent experiments, with three replicates for single concentration (Figures S38-S40).

Compound	CT26	U87	RPE-1	S.I.
2a	4.0 ± 0.5	4.2 ± 0.1	> 100	> 24
2b	4.0 ± 0.3	1.5 ± 0.5	20 ± 5	13
2c	5.7 ± 0.8	10.7 ± 0.7	48 ± 8	4
2d	3.2 ± 0.1	4.4 ± 0.4	> 100	> 23
2e	2.5 ± 0.4	5.5 ± 0.3	> 100	> 18
2f	29 ± 3	11 ± 2	> 100	> 9
4a	11.5 ± 0.2	9.9 ± 0.5	24 ± 7	2.4
4b	4.4 ± 0.4	1.9 ± 0.1	9 ± 2	4.7
4c	45 ± 9	42 ± 5	> 100	> 2.3
2i	*7 ± 1*	*6 ± 1*	*8 ± 2*	*1.3*
2j	*8 ± 1*	*17 ± 1*	*28 ± 2*	*1.6*
1b	> 100		56 ± 21	
1c	> 100		39 ± 16	
cisplatin	2 ± 1	4 ± 1	20.6 ± 0.7	5.2

4. Seahorse Mito Stress Test and NADH catalytic oxidation

It has been largely documented that the diiron vinyliminium structure induces an increased intracellular ROS production, which is mainly responsible for the antiproliferative activity.[28,37,40,41,70] Here, to give additional insight into the mechanism of action of the investigated compounds, the influence on the cellular metabolism was assessed for selected complexes, i.e., **2a**, **2d**, **2e**, **2f**, **4b**, and **4c**. The real time dioxygen consumption rate (OCR) was determined on the CT26 cell line using a Seahorse XF instrument, and the effect on oxidative phosphorylation triggered by ATP production in mitochondria through electron transport chain was evaluated. To determine the influence played by the compounds on the mitochondrial metabolism of the cells, the cells were treated with sequential injections of specific inhibitors of the electron transport chain proteins. In particular, oligomycin was added to inhibit the ATP synthase, FCCP (carbonyl cyanide 4-(trifluoromethoxy)phenylhydrazone) was added as an uncoupling agent that induces maximal OCR, and a combination of Rotenone/Antimycin A was injected to block the electron transport chain, to enable the detection

of non-mitochondrial O_2 consumption. The inhibitors were loaded on the cells, after treatment with the designated complexes and cisplatin at IC_{50} and IC_{25} concentrations, over 24 h. The Mito Stress Test was performed following the Agilent protocol.[71] Briefly, OCR data are in alignment with the antiproliferative activities of the complexes: in particular, cells treated with moderately cytotoxic **2f** and **4c** show a behaviour closer to the control (untreated cells), while cells treated with **2a**, **2d**, **2e** and especially **4b**, which are the most active compounds, exhibit a significantly different OCR profile (Figure 4). This effect becomes more evident after FCCP injection: the ability of the cells to restore the proton balance in the situation of energy demand, triggered by the addition of FCCP, drop drastically; this could be related to the alteration of cell redox homeostasis induced by the compounds. In particular, the OCR profile of **4b** (blue and sky-blue curves in Figure 4) indicates that the basal respiration and the maximal respiration are strongly decreased if compared to non-treated cells (ochre yellow curve).

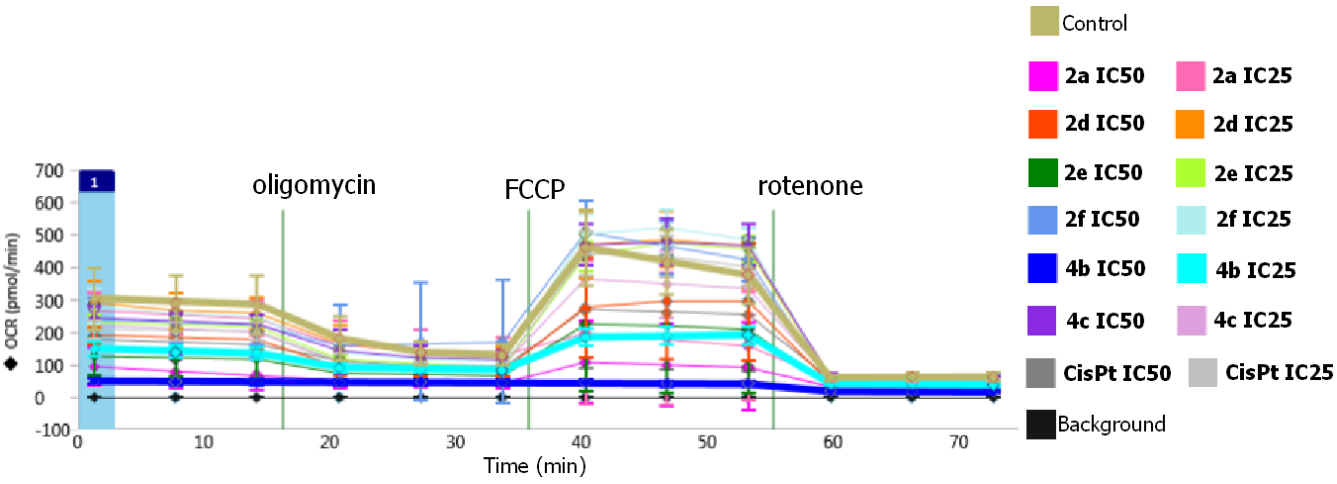

Figure 4. Mito stress test on CT26 cells treated with, respectively, **2a**, **2d**, **2e**, **2f**, **4b**, **4c** and cisplatin. Each line shows the O_2 consumption rate with time of complexes at IC_{25} and IC_{50} concentrations. Lines related to the most effective complex (**4b**) are in bold (blue and sky blue, respectively).

UV-Vis spectroscopy was employed to investigate the ability of **2a** and **2d** to catalyse the aerobic oxidation of the reduced form of nicotinamide adenine dinucleotide (NAD^+), i.e. NADH, in aqueous solution (see Experimental for details). Note that NAD^+ and NADH are important cofactors for the maintenance of redox balance in cells, and changes in the NADH/NAD^+ ratio are correlated with the anticancer activity of diverse transition metal complexes.[72,73] However, both **2a** and **2d** provided TON

values (2a: 3.1, **2d**: 2.2) comparable to that of the reference $FeSO_4$ (3.0), suggesting that direct NADH oxidation is not a preferential route whereby diiron vinyliminium complexes may exert their redox unbalancing power to kill cancer cells.

Conclusions

Iron cyclopentadienyl complexes will hopefully play an important role in the development of future anticancer drugs, and diiron complexes based on the $Fe_2Cp_2(CO)_x$ scaffold have emerged in recent years as interesting additional candidates. Cooperative effects of the bimetallic core allow the building of hydrocarbyl ligands with a broad structural variability, and vinyliminium derivatives constitute an easily accessible family, displaying a promising anticancer potential essentially related to the unbalancing of redox cell homeostasis (ROS production and inhibition of thioredoxin reductase enzyme). To date, over 60 diiron vinyliminium complexes have been assessed for their in vitro antiproliferative activity towards cancer cell lines. Here, we describe the synthesis and characterization of a series of novel diiron vinyliminium complexes with ideal pre-requisites for a drug candidate, such as appreciable water solubility, amphiphilicity and substantial robustness in physiological solution, and their anticancer *in vitro* activity evaluation. We show that the introduction of a cyclohexyl group in a specific position provides a cytotoxic activity comparable to that of cisplatin in CT26 and U87 cancer cells, accompanied by an outstanding selectivity with respect to a non-cancerous cell line (RPE-1). The compounds display a different influence on the mitochondrial metabolism of murine colon cancer cells (CT26), which is correlated to their cytotoxicity. These results supply additional information concerning the structure-activity relationship and the mechanism of action of anticancer diiron vinyliminium complexes.

Experimental

1. Synthesis of diiron complexes

Materials and methods. Organic reactants were purchased from Merck and TCI Europe and were of the highest purity available, while solvents were purchased from Merck. Reactants and solvent were used as received, except THF and CH_2Cl_2 during the synthesis of **3-4**, which were dried with the solvent purification system mBraun MB SPS5. Complexes **1a-d**[33,36] and **2g-h**[37,40] were prepared according to the literature. Unless otherwise stated, reactions and chromatographic purifications were carried out in air and solvents were used from the bottle. Separations were carried out on columns of deactivated alumina (Merck, 4% *w/w* water). Once isolated, products were stored in air. Infrared spectra of solutions were recorded on a Perkin Elmer Spectrum 100 FT-IR spectrometer with a CaF_2 liquid transmission cell (2300-1500 cm^{-1} range). UV-Vis spectra were recorded on an Ultraspec 2100 Pro spectrophotometer. IR and UV-Vis spectra were processed with Spectragryph software.[74] NMR spectra were recorded at 298 K on a Jeol JNM-ECZ500R instrument equipped with a Royal HFX Broadband probe. Chemical shifts (expressed in parts per million) are referenced to the residual solvent peaks (^1H, ^{13}C).[75] NMR spectra were assigned with the assistance of ^1H-^{13}C (*gs*-HSQC and *gs*-HMBC) correlation experiments.[76] NMR signals due to secondary isomeric forms (where it has been possible to detect them) are italicized. Elemental analyses were performed on a Vario MICRO cube instrument (Elementar).

1.1. Synthesis and characterization of diiron vinyliminium complexes 2a-f

General procedure. A solution of **1a-d** (ca. 0.5 mmol) in MeCN (ca. 10 mL) was treated with Me_3NO (1.3 eq.). The resulting mixture was stirred for 1 hour, during which time progressive colour darkening occurred. The complete conversion of the starting material into the corresponding acetonitrile adducts $[Fe_2Cp_2(CO)(\mu\text{-}CO)(NCMe)\{\mu\text{-}CN(Me)(R)\}]CF_3SO_3$ was checked by IR spectroscopy, as is routine for this type of reactions.[77] The volatiles were removed under vacuum to afford a dark-brown residue which was dissolved into dichloromethane (ca. 20 mL) and treated with the appropriate alkyne (ca. 1.4 eq.). The mixture was stirred at

room temperature for 48 hours, then it was chromatographed on an alumina column. Elution with CH_2Cl_2/THF mixtures allowed to separate impurities, then the fraction corresponding to the desired product was isolated. Volatiles were evaporated under reduced pressure, the residue was dissolved in CH_2Cl_2 and diethyl ether/hexane (1:1 v/v) was added. The obtained precipitate was dried under vacuum and isolated as a powder.

$[Fe_2Cp_2(CO)(\mu\text{-}CO)\{\mu\text{-}\eta^1\text{:}\eta^3\text{-}C^3(Cy)C^2HC^1NMe(4\text{-}C_6H_4OMe)\}]CF_3SO_3$, 2a (Figure 5)

Figure 5. Structure of the cation of **2a** (left: *E* isomer; right: *Z* isomer)

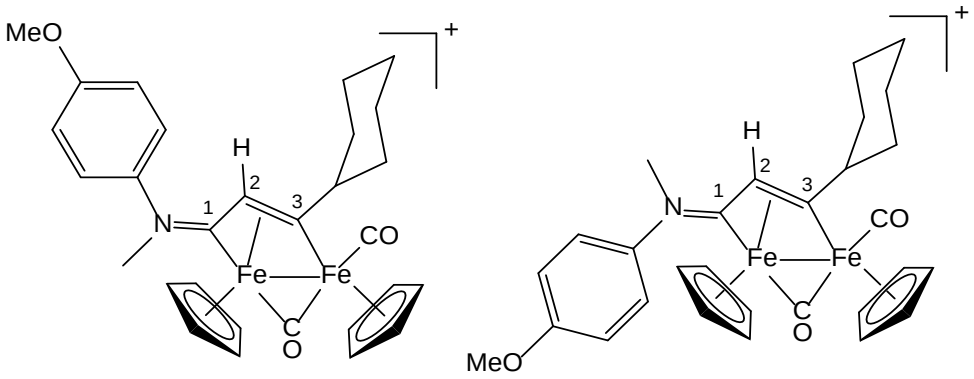

From **1a** (101 mg, 0.162 mmol) and cyclohexyl acetylene. Brown solid, yield 53%. Chromatography: MeCN. Anal. calcd. for $C_{30}H_{32}F_3Fe_2NO_6S$: C, 51.23; H, 4.59; N, 1.99; S, 4.56. Found: C, 51.46; H, 4.69; N, 2.06; S, 4.42. IR (CH_2Cl_2): $\tilde{\nu}/cm^{-1}$ = 1991vs (CO), 1808s (μ-CO), 1640m (C^1N). ^1H NMR (acetone-d_6): δ/ppm = *7.65*, 7.17, *7.23*, 6.92 (d, ^3J = 9.0 Hz, 4H, C_6H_4); 5.56, *5.50*, 5.37, *5.02* (s, 10H, Cp); *5.01*, 4.73 (s, 1H, C^2H); 4.42, *3.95* (s, 3H, NMe); 4.38, *4.35* (m, 1H, CH^{Cy}); 3.79, *3.63* (s, 3H, OMe); 2.61-2.14, 2.01-1.29 (m, 10H, $CH_2{}^{Cy}$). E/Z ratio = 2.5. $^{13}C\{^1H\}$ NMR (acetone-d_6): δ /ppm = 256.6, *256.0* (μ-CO); 230.8, *229.5* (C^1); *221.1*, 220.0 (C^3); *211.8*, 211.7 (CO); *161.2*, 160.7 (arom, C-O), 140.2, *137.4* (arom, N-C), *127.1*, 123.4 (arom, *ortho*-CH), *115.6*, 115.2 (arom, *meta*-CH); 122.5 (q, $^1J_{CF}$ = 322.0 Hz, CF_3SO_3); 92.4, 88.5, *88.1* (Cp); 61.8, *61.7* (CH^{Cy}); *56.2*, 46.9 (NMe); 56.1, *54.4* (OMe); 48.8 (C^2); 41.9, *34.7*, 34.6, *28.4*, 28.3, *27.6*, 27.4, *27.3*, 27.2 ($CH_2{}^{Cy}$). Crystals of **2a** suitable for X-ray analysis were obtained from a CH_2Cl_2 solution layered with Et_2O and settled aside at 4 °C.

$[Fe_2Cp_2(CO)(\mu\text{-}CO)\{\mu\text{-}\eta^1\text{:}\eta^3\text{-}C^3(CH_2Cy)C^2HC^1NMe(4\text{-}C_6H_4OMe)\}]CF_3SO_3$, 2b (Figure 6)

Figure 6. Structure of the cation of **2b** (left: *E* isomer; right: *Z* isomer)

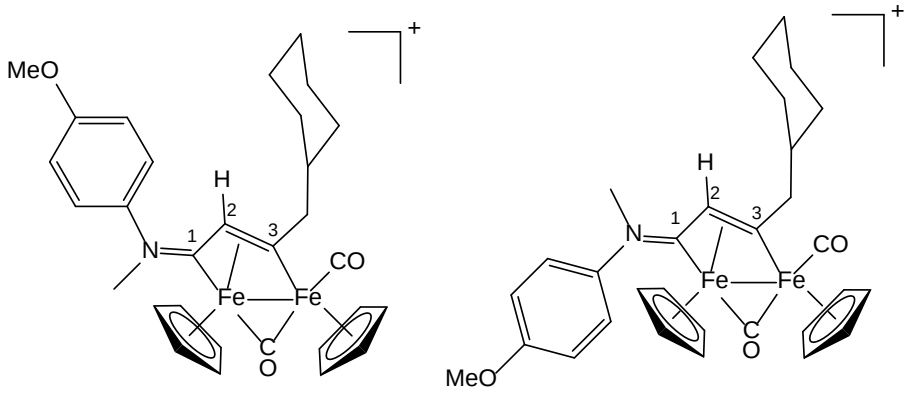

From **1a** (110 mg, 0.177 mmol) and 3-cyclohexyl-1-propyne. Brown solid, yield 83%. Chromatography: MeCN. Anal. calcd. for $C_{31}H_{34}F_3Fe_2NO_6S$: C, 51.90; H, 4.78; N, 1.95; S, 4.47. Found: C, 51.76; H, 4.86; N, 2.01; S, 4.39. IR (CH_2Cl_2): $\tilde{\nu}/cm^{-1}$ = 1989vs (CO), 1810s (μ-CO), 1643m (C^1N). ^1H NMR (acetone-d_6): δ/ppm = *7.65*, 7.20, *7.23*, 6.93 (d, ^3J = 9.0 Hz, 4H, C_6H_4); 5.58, *5.51*, 5.31, 5.00 (s, 10H, Cp); *4.74*, 4.55 (s, 1H, C^2H); *4.52*, 4.50 (dd, J = 12.4 and 3.5 Hz, 1H, CH_2); 4.43, *3.95* (s, 3H, NMe); 3.79, *3.67* (s, 3H, OMe); 3.57 (dd, J =12.4 and 10.2 Hz, 1H, CH_2); 2.22-2.09, 1.90-1.79, 1.50-1.06 (m, 10H, CH_2^{Cy}). E/Z ratio = 3. $^{13}C\{^1H\}$ NMR (acetone-d_6): δ /ppm = 256.5, *255.5* (μ-CO); 231.1, *229.5* (C^1); *213.6*, 213.0 (C^3); *211.7*, 211.6 (CO); *161.2*, 160.7 (arom, C-O), 140.3, *137.0* (arom, N-C), *127.0*, 123.2 (arom, *ortho*-CH), *115.5*, 115.0 (arom, *meta*-CH); 91.7, 88.9, *91.6*, *88.7* (Cp); 63.4 (CH_2); *56.1*, 46.6 (NMe); 56.0, *54.7* (OMe); 54.3, *53.8* (C^2); 43.2, *43.0* (CH^{Cy}); *35.4*, 35.3, *32.8*, 32.5 (CH_2^{Cy}), 27.1 (m, CH_2^{Cy}). Crystals of **3b** suitable for X-ray analysis were obtained from a CH_2Cl_2 solution layered with Et_2O and settled aside at 4 °C.

$[Fe_2Cp_2(CO)(\mu\text{-}CO)\{\mu\text{-}\eta^1\text{:}\eta^3\text{-}C^3(Cy)C^2HC^1NMe(4\text{-}C_6H_4OMe)\}]CF_3SO_3$, 2c (Figure 7)

Figure 7. Structure of the cation of **2c** (left: *E* isomer; right: *Z* isomer)

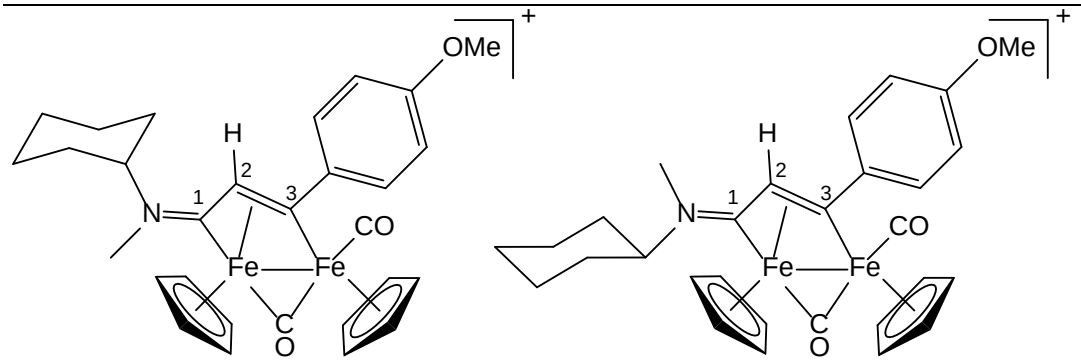

From **1b** and (804 mg, 1.342 mmol) and 4-ethynylanisole. Brown solid, yield 98%. Chromatography: MeCN. Anal. calcd. for $C_{30}H_{32}F_3Fe_2NO_6S$: C, 51.23; H, 4.59; N, 1.99; S, 4.56. Found: C, 51.54; H, 4.41; N, 2.05; S, 4.52. IR (CH_2Cl_2): $\tilde{\nu}/cm^{-1}$ = 1991vs (CO), 1809s (μ-CO), 1658m (C^1N). ^1H NMR (acetone-d_6): δ/ppm = 7.80, 7.09 (d, ^3J = 8.6 Hz, 4H, C_6H_4); 5.38, *5.34*, 5.28, *5.27* (s, 10 H, Cp); *4.92*, 3.77 (tt, J = 11.8 and 3.7 Hz, 1H, CH^{Cy}); 4.70, *4.67* (s, 1H, C^2H); 3.98, *3.32* (s, 3H, NMe); 3.92 (s, 3H, OMe); 2.31-2.28, 1.84-1.07 (m, 10H, $CH_2{}^{Cy}$). Z/E ratio = 1.3. $^{13}C\{^1H\}$ NMR (acetone-d_6): d/ppm = *258.0*, 257.1 (μ-CO); *225.7*, 224.9 (C^1); 211.4, *211.2* (CO); 205.2 (C^3); 159.8 (arom, C-O), 150.4 (arom, C^3-C), 129.9 (arom, *ortho*-CH), 114.4 (arom, *meta*-CH); 122.5 (q, $^1J_{CF}$ = 322.1 Hz, CF_3SO_3); 92.7, 88.8, *88.6* (Cp); 76.4, *68.8* (CH^{Cy}); 55.8 (OMe); *53.2*, 52.6 (C^2); *44.1*, 38.9 (NMe); 26.1, 25.6, 25.4 ($CH_2{}^{Cy}$). Crystals of **3c** suitable for X-ray analysis were obtained from a CH_2Cl_2 solution layered with Et_2O and settled aside at 4 °C.

$[Fe_2Cp_2(CO)(\mu\text{-}CO)\{\mu\text{-}\eta^1\text{:}\eta^3\text{-}C^3(Cy)C^2HC^1NMe(Cy)\}]CF_3SO_3$, 2d (Figure 8)

Figure 8. Structure of the cation of **2d** (left: *E* isomer; right: *Z* isomer)

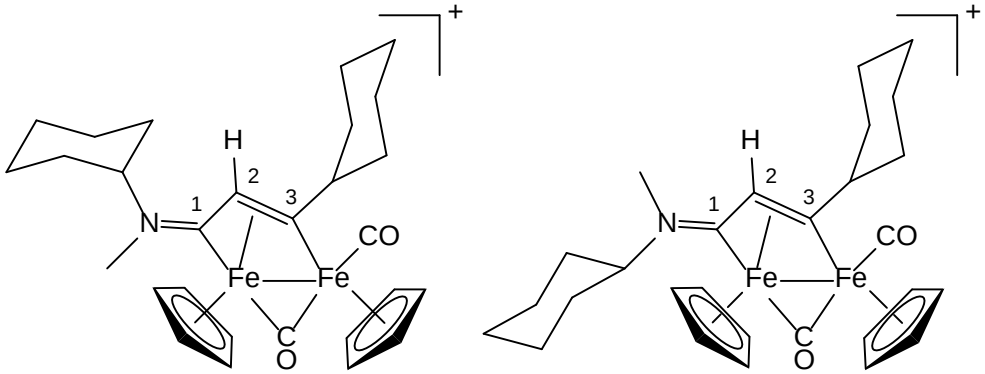

From **1b** (153 mg, 0.255 mmol) and cyclohexyl acetylene. Brown solid, yield 78%. Chromatography: MeCN. Anal. calcd. for $C_{29}H_{36}F_3Fe_2NO_5S$: C, 51.27; H, 5.34; N, 2.06; S, 4.72. Found: C, 51.45; H, 5.23; N, 2.09; S, 4.62. IR (CH_2Cl_2): $\tilde{\nu}/cm^{-1}$ = 1989vs (CO), 1805s (μ-CO), 1659m (C^1N). ^1H NMR (acetone-d_6): δ/ppm = 5.49, 5.48, 5.25, 5.21 (s, 10 H, Cp); 4.83, 4.36, 3.55 (m, 2H, CH^{Cy}); 4.79, 4.77 (s, 1H, C^2H); 3.92, 3.16 (s, 3H, NMe); 2.85-2.26, 1.99-1.35 (m, 20H, $CH_2{}^{Cy}$); E/Z ratio ≈ 1. $^{13}C\{^1H\}$ NMR (acetone-d_6): d/ppm = 258.4, 257.6 (μ-CO); 226.0, 225.0 (C^1); 219.6, 219.3 (C^3); 212.0, 211.7 (CO); 122.5 (q, $^1J_{CF}$ = 322.2 Hz, CF_3SO_3); 92.0, 87.9, *87.7* (Cp); 76.0, 68.8, 61.6, 61.4 (CH^{Cy}); 46.8, 46.0 (C^2); 43.5, 38.8 (NMe); 42.0, 41.9, 34.5, 30.7, 30.6, 28.3, 27.4, 27.3, 27.2, 26.1, 25.6, 25.5, 25.3 ($CH_2{}^{Cy}$).

A variable temperature ^1H NMR experiment conducted on a CD_3CN solution of **2d**, up to 75 °C, did non evidence any change in the isomer ratio.

$[Fe_2Cp_2(CO)(\mu\text{-}CO)\{\mu\text{-}\eta^1\text{:}\eta^3\text{-}C^3(Cy)C^2HC^1NMe(CH_2Ph)\}]CF_3SO_3$, 2e (Figure 9)

Figure 9. Structure of the cation of **2e** (left: *E* isomer; right: *Z* isomer)

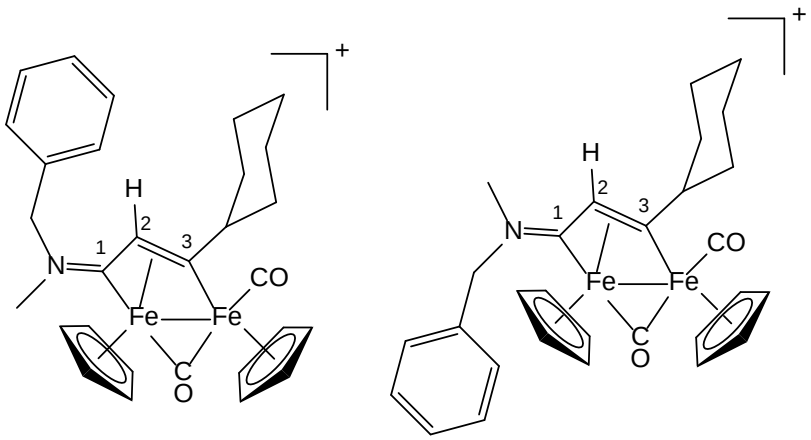

From **1c** (107 mg, 0.176 mmol) and cyclohexyl acetylene. Brown solid, yield 69%. Chromatography: MeCN. Anal. calcd. for $C_{30}H_{32}F_3Fe_2NO_5S$: C, 52.42; H, 4.69; N, 2.04; S, 4.67. Found: C, 52.31; H, 4.77; N, 1.97; S, 4.79. IR (CH_2Cl_2): $\tilde{\nu}/cm^{-1}$ = 1990vs (CO), 1803s (μ-CO), 1667m (C^1N). ^1H NMR (acetone-d_6): δ/ppm = 7.46-7.26 (m, 5H, Ph), *5.55*, 5.52, 5.29 (s, 10H, Cp); *5.63*, *5.54*, 4.77, 4.66 (d, ^2J = 14.0 Hz, 1H, CH_2); *4.90*, 4.79 (s, 1H, C^2H); 4.39 (m, 1H, (CH^{Cy}); 3.85, *3.07* (s, 3H, NMe); 2.60-2.07, 1.79-1.29 (m, 10H, $CH_2{}^{Cy}$). E/Z ratio = 2. $^{13}C\{^1H\}$ NMR (acetone-d_6): δ/ppm = 258.6, *257.4* (μ-CO); 228.3, *228.1* (C^1); *220.2*, 219.8 (C^3); *211.8*, 211.7 (CO);

134.3, 133.7 (arom, CH_2-C), 130.0, 129.9, 129.7 (arom, CH); 122.5 (q, $^1J_{CF}$ = 322.0 Hz, CF_3SO_3); *92.2*, 92.1, 88.0 (Cp); 68.7, *62.2* (CH_2); 61.6 (CH^{Cy}); *48.0*, 42.8 (NMe); *47.5*, 47.3 (C^2); *42.0*, 41.8, *34.6*, 34.6, 28.4, 27.5, 27.3 ($CH_2{}^{Cy}$).

$[Fe_2Cp_2(CO)(\mu\text{-}CO)\{\mu\text{-}\eta^1\text{:}\eta^3\text{-}C^3(4\text{-}C_6H_4OMe)C^2HC^1NMe_2)\}]CF_3SO_3$, 2f (Figure 10)

Figure 10. Structure of the cation of **2f**

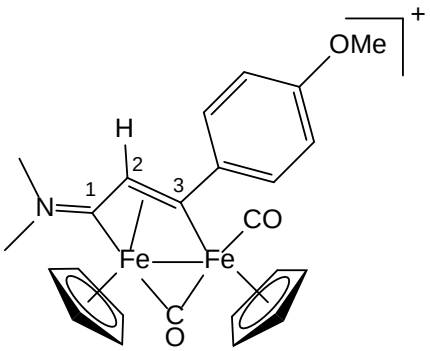

From **1d** (213 mg, 0.401mmol) and 4-ethynylanisole. Green solid, yield 93%. Chromatography: MeCN. Anal. calcd. for $C_{25}H_{24}F_3Fe_2NO_6S$: C, 47.27; H, 3.81; N, 2.21; S, 5.05. Found: C, 47.11; H, 3.88; N, 2.16; S, 4.95. IR(CH_2Cl_2): $\tilde{\nu}$/cm^{-1} = 1990vs (CO), 1806s (μ-CO), 1680m (C^1N). ^1H NMR (acetone-d_6): δ/ppm = 7.81, 7.09 (d, ^3J = 8.7 Hz, 4H, C_6H_4); 5.36, 5.26 (s, 10H, Cp); 4.60 (s, 1H, C^2H); 4.02, 3.92 (s, 6H, NMe_2); 3.44 (s, 3H, OMe). $^{13}C\{^1H\}$ NMR (acetone-d_6): δ/ppm = 257.2 (μ-CO); 226.2 (C^1); 211.1 (CO); 204.8 (C^3); 159.8 (arom, C^3-C); 150.1 (arom, C-O); 129.8 (arom, *ortho*-CH); 122.4 (q, $^1J_{CF}$ = 322.2 Hz, CF_3SO_3); 114.4 (arom, *meta*-CH); 92.4, 88.6 (Cp); 55.7, 45.0 (NMe_2); 53.5 (C^2); 51.7 (OMe).

1.2. Synthesis and characterization of hydrazone-decorated vinyliminium complexes 4a-c

General procedure. A solution of the selected vinyliminium complex (**2c,g,h**; ca. 0.12 mmol) in anhydrous THF (ca. 20 mL) was treated with N_2CHCO_2Et (5 eq.) and NaOMe (3-4 eq.), and stirring under N_2 atmosphere was maintained for 1 hour. Quick filtration of the resulting green solution through an alumina column was performed with THF as eluent. After removal of the volatiles, a more careful

chromatography on an alumina column afforded a green band corresponding to **3a-c** (eluent: THF/MeOH mixture). Solutions of **3a-b** (from **2c,g**) in anhydrous CH_2Cl_2 (ca. 20 mL) were characterized by IR spectroscopy [**3a**, $\tilde{\nu}$/cm^{-1} = 1958vs (CO), 1771s (μ-CO), 1703m (OCO), 1602w (C^4=N), 1504w (C^1N); **3b**, $\tilde{\nu}$/cm^{-1} = 1959vs (CO), 1772s (μ-CO), 1682m (OCO), 1594w (C^4=N), 1579w (C^1N)] and each solution was then treated with 4-10 eq. of methyl iodide while stirring under N_2 atmosphere. After 24-48h, IR analysis on an aliquot of the red solution indicated the complete consumption of **3a-b**. Hence, after removing the volatiles under reduced pressure, a mixture of the residue and $AgNO_3$ (ca. 1.2 eq. with respect to starting vinyliminium complex) in methanol (ca. 15 mL) was stirred for 2 hours. The solvent was evaporated, and a dichloromethane solution of the solid was filtered through celite. The solvent was removed under reduced pressure and the residue was washed with diethyl ether and hexane; **4a-b** were finally obtained as air-stable powders after drying under vacuum.

Complex **3c** was isolated as follows. The reaction mixture obtained from **2h** (ca. 250 mg), ethyl diazoacetate and sodium methoxide was quickly filtered through a short alumina pad using THF and then MeCN as eluent. Volatiles were evaporated from the filtrated solution under reduced pressure. The obtained residue was dissolved in the minimum volume of CH_2Cl_2, and this solution was charged on alumina. Elution with CH_2Cl_2 and CH_2Cl_2/THF (2:1 v/v) allowed to separate impurities, then an emerald-green fraction was collected using neat THF as eluent. Removal of the solvent under vacuum afforded **3c** as a dark-green solid. Yield 72%. IR (CH_2Cl_2): $\tilde{\upsilon}$/cm^{-1} = 1960vs (CO), 1775s (μ-CO), 1711s (OCO), 1589m (C^4=N). ^{1}H NMR (CD_2Cl_2): δ/ppm = 7.80, 7.61, 7.46, 7.21, 6.96 (m, 5 H, Ph); *6.57*, 6.47 (s, 1 H, C^4H); 4.88, *4.74*, *4.66*, 4.53 (s, 10 H, Cp); 4.12 (br, 2 H, C$\underline{H}_2$CH$_3$); 3.79, 3.08, *2.68, 2.61* (s, 6 H, NMe_2); 1.26 (br, 3 H, $CH_2C\underline{H}_3$). Isomer ratio = 2.3.

To obtain **4c**, methyl triflate was directly added dropwise to a solution of **3c** in dichloromethane. The resulting solution was stirred at room temperature for 3 h and then charged on an alumina column; **4c**

was collected as a brown fraction using a THF/MeCN mixture (1:1 *v/v*) as eluent, and isolated upon drying under vacuum.

$[Fe_2Cp_2(CO)(\mu\text{-}CO)\{\mu\text{-}\eta^1\text{:}\eta^3\text{-}C^3(4\text{-}C_6H_4OMe)C^2(NMeN{=}CHCO_2Et)C^1NMe(Cy)\}]NO_3$, 4a (Figure 11)

Figure 11. Structure of the cation of **4a** (left: *Z* isomer; right: *E* isomer).

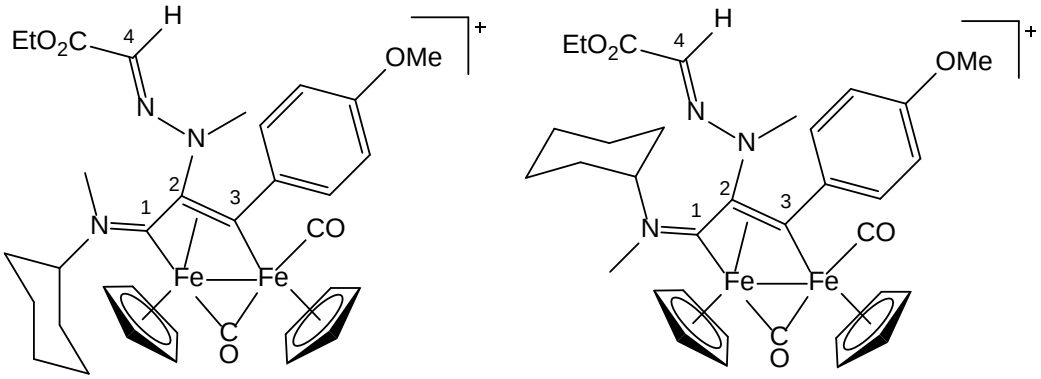

From **2c** (76 mg, 0.108 mmol), CH_3I and $AgNO_3$. Dark-red solid, yield 67%. Anal. calcd. for $C_{34}H_{40}Fe_2N_4O_8$: C, 54.86; H, 5.42; N, 7.53. Found: C, 55.16; H, 5.37; N, 7.63. IR (CH_2Cl_2): ν/cm^{-1} = 1991vs (CO), 1812s (μ-CO), 1703m (OCO), 1603m (C^1=N), 1563w (C^4=N). ^{1}H NMR (acetone-d_6): δ/ppm = 7.96-7.03 (m, 4H, C_6H_4); 6.57, *6.42* (s, 1H, C^4H); *5.66*, 5.59, *5.33*, 5.29 (s, 10H, Cp); 4.80, *3.28* (m, 1H, CH^{Cy}); 4.22 (m, 2H, CH_2^{Et}); 3.94, *3.01* (s, 3H, C^1NMe); 3.91, *3.90* (s, 3H, OMe); 2.8 (s, 3H, C^2NMe); 2.35-2.21, 1.92-1.57, 1.22-1.06 (m. 10H, CH_2^{Cy}); 1.30 (m, 3H, CH_3^{Et}). Isomer ratio = 1.5. ^{13}C{^{1}H} NMR (acetone-d_6): δ /ppm = 256.7 (μ-CO); *224.7*, 222.9 (C^1); *211.8*, 211.6 (CO); *204.5*, 202.6 (C^3); *164.2*, 164.1 ($\underline{C}O_2Et$); 159.5 (arom, C-O), 145.2, *145.0* (arom, C^3-C); 133.1, 126.5, 126.2, 114.6 (arom, CH); 123.1, 121.3 (C^4); 93.3, *90.4*, 89.9 (Cp); 89.9 (C^2); *75.7*, 68.8 (CH^{Cy}); 61.1, *60.9* (CH_2^{Et}); 55.8 (OMe); 42.3, *38.0* ($C^1N\underline{Me}$); 39.1, 38.1 ($C^2N\underline{Me}$); 30.8, 30.7, 30.6, 26.1, 25.8, 25.7, 25.6, 25.5, 25.3 (CH_2^{Cy}); 14.7 (CH_3^{Et}).

$[Fe_2Cp_2(CO)(\mu\text{-}CO)\{\mu\text{-}\eta^1\text{:}\eta^3\text{-}C^3(Ph)C^2(NMeN{=}CHCO_2Et)C^1N(CH_2Ph)_2\}]NO_3$, 4b (Figure 12)

Figure 12. Structure of the cation of **4b**.

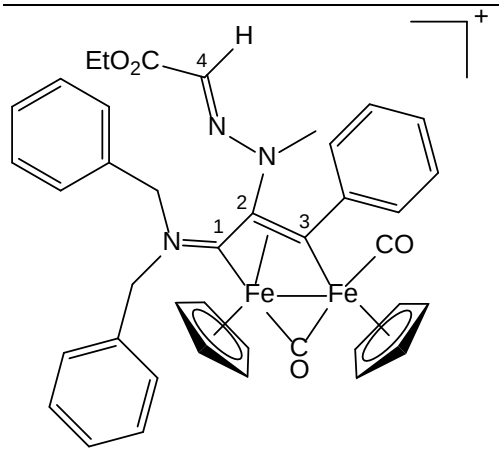

From **2g** (94 mg, 0.124 mmol), CH_3I and $AgNO_3$. Dark-red solid, yield 53%. Anal. calcd. for $C_{40}H_{38}Fe_2N_4O_7$: C, 60.17; H, 4.80; N, 7.02. Found: C, 60.01; H, 4.72; N, 6.94. IR (CH_2Cl_2): $\tilde{\nu}/cm^{-1}$ = 1992vs (CO), 1816s (μ-CO), 1709m (OCO), 1626m (C^1=N), 1558w (C^4=N). ^1H NMR (acetone-d_6): δ/ppm = 7.88-6.76 (m, 15H, Ph); 6.41 (s, 1H, C^4H); 5.76, 5.41 (s, 10H, Cp); 5.75, 5.25 (d, ^2J = 15.1Hz, 2H, CH_2Ph); 4.61, 4.40 (d, ^2J = 14.9 Hz, 2H, CH_2Ph); 4.35 (q, ^3J = 7.1 Hz, 2H, CH_2^{Et}); 2.84 (s, 3H, C^2NMe); 1.35 (t, ^3J = 7.1 Hz, 3H, CH_3^{Et}). $^{13}C\{^1H\}$ NMR (acetone-d_6): δ /ppm = 255.1 (μ-CO); 228.7 (C^1); 211.6 (CO); 203.0 (C^3); 164.3 (CO_2); 152.6 (arom, C^3-Ph); 133.6 (arom, CH_2-Ph), 132.2, 132.0. 129.9, 129.7, 129.6, 129.5, 129.4, 128.6, 127.9, 125.0 (arom, CH); 122.1 (C^4); 95.8, 90.7 (Cp); 90.7* (C^2); 64.3, 59.3 ($\underline{C}H_2Ph$); 61.2 (CH_2^{Et}); 39.1 ($C^2N\underline{Me}$); 14.8 (CH_3^{Et}). *Hidden by Cp signal, assigned by HMBC.

$[Fe_2Cp_2(CO)(\mu\text{-}CO)\{\mu\text{-}\eta^1\text{:}\eta^3\text{-}C^3(Ph)C^2(NMeN{=}CHCO_2Et)C^1NMe_2\}]CF_3SO_3$, 4c (Figure 13)

Figure 13. Structure of the cation of **4c**.

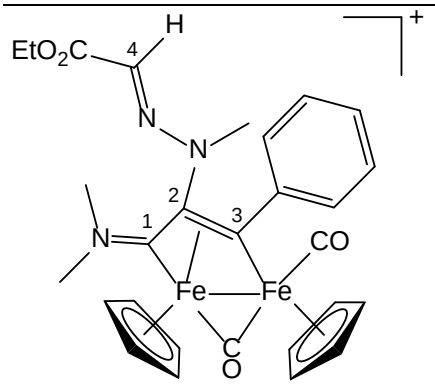

From **2h** (250 mg, 0.413 mmol) and CF_3SO_3Me. Brown solid, yield 62%. Anal. calcd. for $C_{29}H_{30}F_3Fe_2N_3O_7S$: C, 47.50; H, 4.12; N, 5.73; S, 4.37. Found: C, 47.62; H, 4.02; N, 5.60; S, 4.31. IR (CH_2Cl_2): $\tilde{\nu}$/cm^{-1} = 1995vs (CO), 1815s (μ-CO), 1709m (OCO), 1667m (C^1=N), 1568w (C^4=N). ^{1}H NMR ($CDCl_3$): δ/ppm = 7.56-7.31 (m, 5 H, Ph); 6.41 (s, 1 H, C^4H); 5.32, *5.19*, *5.14*, 4.96 (s, 10 H, Cp); 4.22 (q, ^{3}J = 7.1 Hz, 2 H, CH_2^{Et}); 3.88, 3.11 (s, 6H, C^1NMe_2); 2.66 (s, 3 H, C^2NMe); 1.30 (t, ^{3}J = 7.1 Hz, 3 H, CH_3^{Et}). $^{13}C\{^1H\}$ NMR ($CDCl_3$): δ/ppm = 254.6 (μ-CO); 224.6 (C^1); 210.0 (CO); 191.2 (C^3); 163.4 (CO_2); 151.6 (arom, C^3-Ph); 129.8-124.4 (arom, CH); 122.7 (C^4); 92.3, 88.7 (Cp); 83.8 (C^2); 61.0 (CH_2^{Et}); 50.5, 45.2 ($C^1N\underline{Me_2}$); 37.6 ($C^2N\underline{Me}$); 14.4 (CH_3^{Et}).

3. X-ray crystallography

Crystal data and collection details for **2a**, **2b** and **2c** are reported in Table 4. Data were recorded on a Bruker APEX II diffractometer equipped with a PHOTON2 detector using Mo–Kα radiation. The structures were solved by direct methods and refined by full-matrix least-squares based on all data using F^2.[78] Hydrogen atoms were fixed at calculated positions and refined isotropically using a riding model,

Table 4. Crystal data and measurement details for **2a**, **2b** and **2c**.

	2a	**2b**	**2c**
Formula	$C_{30}H_{32}F_3Fe_2NO_6S$	$C_{31}H_{34}F_3Fe_2NO_6S$	$C_{31}H_{34}Cl_2F_3Fe_2NO_6S$
FW	703.32	717.35	788.25
T, K	100(2)	100(2)	100(2)
λ, Å	0.71073	0.71073	0.71073

Crystal system	Monoclinic	Monoclinic	Monoclinic
Space group	$P2_1/n$	$P2_1/n$	$P2_1/n$
a, Å	8.9184(4)	9.2150(14)	12.127(3)
b, Å	25.5418(12)	25.306(4)	14.583(3)
c, Å	13.6066(6)	13.712(2)	19.147(4)
α,°	90	90	90
β,°	103.8370(10)	107.023(5)	102.868(6)
γ,°	90	90	90
Cell Volume, Å^3	3009.5(2)	3057.5(8)	3301.1(12)
Z	4	4	4
D_c, g·cm^{-3}	1.552	1.558	1.586
μ, mm^{-1}	1.096	1.080	1.165
F(000)	1448	1480	1616
Crystal size, mm	0.16×0.14×0.11	0.21×0.12×0.09	0.18×0.12×0.08
θ limits,°	1.735-25.099	1.609-25.198	1.772-25.047
Reflections collected	39165	30214	31684
Independent reflections	5364 [R_{int} = 0.0435]	5403 [R_{int} = 0.0908]	5768 [R_{int} = 0.1935]
Data / restraints /parameters	5364 / 0 / 390	5403 / 6 / 399	5738 / 60 / 417
Goodness on fit on F^2 [a]	1.151	1.245	1.253
R_1 ($I > 2\sigma(I)$) [b]	0.0426	0.0772	0.1418
wR_2 (all data) [c]	0.0918	0.1534	0.3018
Largest diff. peak and hole, e Å^{-3}	0.610 / –0.356	0.939 / –0.621	1.534 / –0.532

[a] Goodness on fit on $F^2 = [\Sigma w(F_O^2 - F_C^2)^2/(N_{ref} - N_{param})]^{1/2}$, where $w = 1/[\sigma^2(F_O^2) + (aP)^2 + bP]$, where $P = (F_O^2 + 2F_C^2)/3$; N_{ref} = number of reflections used in the refinement; N_{param} = number of refined parameters. [b] $R_1 = \Sigma||F_O| - |F_C||/\Sigma|F_O|$. [c] $wR_2 = [\Sigma w(F_O^2 - F_C^2)^2/\Sigma w(F_O^2)^2]^{1/2}$, where $w = 1/[\sigma^2(F_O^2) + (aP)^2 + bP]$, where $P = (F_O^2 + 2F_C^2)/3$.

4. Behaviour of the diiron complexes in aqueous media

4.1. Solubility in D_2O.

4.1.1. NMR method. A suspension of the selected diiron complex (*ca*. 3 mg) in a D_2O solution (0.5 mL) containing dimethylsulfone ($DMSO_2$) as internal standard ($1.013 \cdot 10^{-2}$ M) was vigorously stirred at room temperature for 30 minutes. The saturated solution was filtered over celite, transferred into an NMR tube and analysed by ^{1}H NMR (delay time = 4s; number of scans = 25). The concentration of the saturated solution (= solubility) was calculated by the relative integral with respect to $DMSO_2$ (δ/ppm = 3.16, s). Results are compiled in Table 2.

4.1.2. ICP-OES method. The selected diiron complex was dissolved in deionised water (H_2O or D_2O) up to saturation. The mixture was filtered, resulting in a pale brown-yellow solution. Then, 5 mL of HNO_3 65% and 21 mL of H_2O_2 30% solutions were added. After 24 h, the volume of the colourless solution was diluted to 50

mL by addition of MilliQ water. The final solution was analysed through ICP-OES using a ThermoFisher ICAP 7200 instrument (Argon as auxiliary gas). A blank experiment was performed using 2 mL of MilliQ water as a sample. Each measurement was executed in triplicate. Iron was determined at three different wavelengths (λ = 259.940 nm, axial; 238.204 nm, radial; 239.562 nm, radial).

4.1.3. UV-Vis method. A stock solution of the selected complex in DMSO was prepared. Aliquots of this solution were diluted with H_2O or D_2O to obtain standard solutions with known concentrations (max. 1% *v/v* of DMSO). The solutions were analysed by UV-Vis spectroscopy to make a calibration line. Then, a saturated solution of the complex in H_2O or D_2O was filtered and analysed via UV-Vis allowing to determine the solubility concentration.

4.2. Stability in aqueous solutions. The selected diiron complex (*ca*. 3-4 mg) was dissolved in a D_2O/DMSO-d_6 solution containing $DMSO_2$. The mixture was stirred for 30 minutes, filtered over celite and transferred into an NMR tube. The solution (C_{Fe} = 6 $\square^{-3}$ M) was analysed by ^{1}H NMR (delay time = 4 s; number of scans = 25, see Table S2) then heated at 37 °C for 72 h. After cooling to room temperature, the final solution was separated from a little amount of a brown solid[79] by filtration over celite and the ^{1}H NMR spectrum was recorded. In each case, no new {FeCp} species was identified. The residual amount of starting material in solution (% with respect to the initial spectrum) was calculated by the relative integral with respect to $DMSO_2$ as internal standard (Table 2). The same procedure was adopted after dissolving the selected diiron complex (*ca*. 3-4 mg) in DMEM-d/DMSO-d_6 solution containing a measured amount of $DMSO_2$.[80]

4.3. Determination of partition coefficients (Log P_{ow}). Partition coefficients (P_{ow}; IUPAC: K_D partition constant[81]), defined as $P_{ow} = c_{org}/c_{aq}$, where c_{org} and c_{aq} are the molar concentrations of the selected complex in the organic and aqueous phases, respectively, were determined by the shake-flask method and UV-Vis measurements.[80,82] All the operations were carried out at 21±1 °C. De-ionized water and 1-octanol were mixed and vigorously stirred for 24 hours at ambient temperature to allow saturation of both phases, then separated by centrifugation and used for the following experiments. A stock solution of the selected diiron complex (*ca.* 4 mg) was prepared by first adding acetone (20 μL, to help solubilization), followed by water-saturated octanol (4.0 mL). The solution was diluted with water-saturated octanol, so that $1.0 \leq A \leq 2.0$ at the

selected wavelength, and its UV-Vis spectrum was recorded (A^0_{org}). An aliquot of the solution (V_{org} = 1.2 mL) was transferred into a test tube and octanol-saturated water ($V_{org} = V_{aq}$ = 1.2 mL) was added. The mixture was vigorously stirred for 30 min at room temperature then centrifuged (5000 rpm, 10 min). The UV-Vis spectrum of the organic phase was recorded (A^f_{org}) and the partition coefficient was calculated as $P_{ow} = (A^f_{org} – A_{bkg})/(A^0_{org} - A^f_{org})$ where A^0_{org} and A^f_{org} are the absorbance in the organic phase before and after partition with the aqueous phase, respectively, while A_{bkg} is the absorbance of the organic solvent. The absorbance at a selected wavelength (shoulder band or inflection point) was used for quantitation. The procedure was repeated three times for each sample (from the same stock solution); results are given as mean ± standard deviation (Table 2).

5. Evaluation of the anticancer potential

5.1. Cell culture and cytotoxicity studies. CT26 (mouse colon carcinoma) and U87 (human glioblastoma) cells were cultured in DMEM medium (Gibco). RPE-1 (non-cancerous retinal pigment epithelial cell) were cultured in DMEM-F12 medium (Gibco). All the culture media were supplemented with 10% foetal bovine serum (Gibco) and 1% PenStrep (Gibco). Cells were maintained in a humidified atmosphere at 37°C and 5% CO_2. CT26 and U87 cells were seeded at a 4.000 cells/well density in flatbottom 96-well plates (100 µL/well), while RPE-1 were seeded at 6.000 cells/well density. After seeding, cells were incubated at 37°C for 15-24 h to allow the cells to attach to the bottom of the wells. Stock solutions of the diiron compounds were prepared in DMSO and rapidly diluted in the medium (1% DMSO content maximum). The stock solution of the reference drug cisplatin was prepared in saline solution, NaCl 0.9% w/v. The medium was replaced by dilutions of tested compounds in a fresh medium (100 µL/well) to obtain the following concentration range: 0.01, 0.03, 0.1, 0.3, 1, 3, 10, 30, and 100 µM for the tested compounds and for the reference drug cisplatin. After loading the drug, cells were incubated for 48 h at 37°C. The medium was then replaced with 100 µL of a fresh medium containing resazurin (0.2 mg/mL) and incubated for 4 h. The florescence of the wells, directly proportional to the number of survived cells, was determined by reading the plates using a BioTeck Cytation5 Imaging Reader (λ_{exc} = 540 nm; λ_{read} = 590 nm). Fluorescence data were normalized by attributing 100% cell viability to the mean signal obtained for the non-treated cells and 0% to the signal obtained from wells containing the

highest drug concentration. Data were fitted using GraphPad Prism Software (v6) and IC_{50} values were calculated by nonlinear regression. All experiments were performed in triplicates and the IC_{50} values are listed in Table 3.

5.2. Seahorse Mito stress test. CT26 cells were seeded in Seahorse XFe96 well plate at density of 40.000 cells per well in 80 µl. After 24 h cells were treated with IC_{50} and IC_{25} concentration of complexes **2a**, **2d**, **2e**, **2f**, **4b**, **4c** and cisplatin. Untreated cells were used as control. After 24 h of incubation, the drug-containing medium was carefully removed from the wells and the cells were washed thrice using bicarbonate and serum free S18 DMEM, supplemented with glucose (1.8 mg/ mL), 1% glutamine and 1% sodium pyruvate, and incubated in a non-CO_2 incubator at 37 °C for 1h. Mito Stress assay was run using Oligomycin 1 µM, FCCP 1 µM and mixture of Antimycin-A 1 µM / Rotenone 1 µM each in ports A, B and C respectively, using Seahorse XFe96 Extracellular Flux Analyzer.

5.3. Dynamic Light Scattering. Stock solutions (2 mM) of selected complexes in DMSO were filtered on a 0.22 µm membrane and were diluted at a concentration of 5 µM and 20 µM, respectively, in filtered PBS containing 10% of FBS. The nanoparticle size distributions by intensity were then determined by dynamic light scattering (DLS) using a Malvern ZetaSizer Nano ZS (scattering angle = 173°) at a temperature of 25 °C with an equilibrium time of 120 s. Data are compiled in Table S3.

5.4. Catalytic NADH oxidation. NADH was stored at −20°C under N_2; a stock NADH solution (2.3×10^{-4} mol·L^{-1}) was prepared in phosphate-buffered aqueous solution (Na_2HPO_4/NaH_2PO_4; 5.5×10^{-3} mol·L^{-1}, pH = 7.2) and stored at 4°C. Stock solutions of diiron complexes (**2a**, **2d**; 2.0×10^{-4} mol·L^{-1}) were prepared in DMSO immediately before use. $FeSO_4$ was used as a reference compound (stock solution prepared in H_2O). Solutions of each diiron compound (0.35 mL) and NADH (6.6 mL) were mixed, resulting in a 5% DMSO aqueous solution containing 2.2×10^{-4} M NADH and 1.0×10^{-5} M diiron compound (4.5% mol/mol). The solution was stirred at 37 °C for 24 h and periodically analysed by UV–Vis spectroscopy (260–600 nm) using PMMA cuvettes (1.0 cm path-length). Turnover numbers were calculated as $TON = c(0)/c_{Fe} \cdot [A(0) - A(t)]/A(0)$ where A is the absorbance at λ_{max} = 339 nm, and c(0) and c_{Fe} are the initial molar concentrations of NADH and the selected diiron compound, respectively.

Acknowledgements

We gratefully thank the University of Pisa (PRA_2020_39: "New horizons in CO_2 chemistry: from capture to fine chemicals and metal-based drugs") and the European Union's Horizon 2020 research and innovation program (Marie Skłodowska-Curie Innovative Training Network Nature-ETN, H2020-MSCA-ITN-2019-861381) for financial support. This work was financially supported by an ERC Consolidator Grant PhotoMedMet to G.G. (GA 681679) and has received support under the program *Investissements d'Avenir* launched by the French Government and implemented by the ANR with the reference ANR-10-IDEX-0001-02 PSL (G.G.).

Conflicts of interest

The authors declare no competing financial interests.

Author contributions

S.B.: synthesis and characterization of diiron complexes and biological studies; M.D.P.: biological studies and supervision; L.B.: characterization of diiron complexes and funding; S.Z.: resolution of X-ray structures; G.G. and F.M.: supervision, funding and writing.

Supporting Information Available

NMR spectra of products (major isomer: blue signals; minor isomer: red signals); water solubility data; IC_{50} plots; dynamic light scattering data. CCDC reference numbers 2232357 (**2a**), 2232358 (**2b**) and 2232359 (**2c**) contain the supplementary crystallographic data for the X-ray studies reported in this work. These data are available free of charge at www.ccdc.cam.ac.uk/conts/retrieving.html (or from the Cambridge Crystallographic Data Centre, 12, Union Road, Cambridge CB2 1EZ, UK; e-mail: deposit@ccdc.cam.ac.uk).

References

1 E. J. Anthony, E. M. Bolitho, H. E. Bridgewater, O. W. L. Carter, J. M. Donnelly, C. Imberti, E. C. Lant, F. Lermyte, R. J. Needham, M. Palau, P. J. Sadler, H. Shi, F.-X. Wang, W.-Y. Zhang, Z. Zhang, Metallodrugs are unique: opportunities and challenges of discovery and development. Chem. Sci., 2020, 11, 12888–12917.

2 M. Marloye, G. Berger, M. Gelbcke, A survey of the mechanisms of action of anticancer transition metal complexes. Future Med. Chem. 2016, 8, 2263-2286.

3 E. Boros, P. J. Dyson, G. Gasser, Classification of Metal-Based Drugs according to Their Mechanisms of Action. Chem 2020, 6, 41–60.

4 K. L. Haas, K. J. Franz. Application of Metal Coordination Chemistry To Explore and Manipulate Cell Biology. Chem. Rev. 2009, 109, 4921–4960.

5 S. Ghosh, Cisplatin: The first metal based anticancer drug, Bioorg. Chem. 2019, 88, 102925.

6 S. Dilruba, G. V. Kalayda, Platinum-based drugs: past, present and future. Cancer Chemother. Pharmacol. 2016, 77, 1103–1124.

7 R. C. Todd, S. J. Lippard, Inhibition of transcription by platinum antitumor compounds, Metallomics, 2009, 1, 280–291.

8 R. Oun, Y. E. Moussa, N. J. Wheate, The side effects of platinum-based chemotherapy drugs: a review for chemists. Dalton Trans. 2018, 47, 6645–6653.

9 L. Qi, Q. Luo, Y. Zhang, F. Jia, Y. Zhao, F. Wang, Advances in Toxicological Research of the Anticancer Drug Cisplatin, Chem. Res. Toxicol. 2019, 32, 1469−1486.

10 K. Peng, B.-B. Liang, W. Liu, Z.-W. Mao, What blocks more anticancer platinum complexes from experiment to clinic: Major problems and potential strategies from drug design perspectives. Coord. Chem. Rev. 2021, 449, 214210.

11 B. S. Murray, P. J. Dyson, Recent progress in the development of organometallics for the treatment of cancer. Curr. Opinion Chem. Biol. 2020, 56, 28-34.

12 P. Zhang, P. J. Sadler, Advances in the design of organometallic anticancer complexes. J. Organomet. Chem. 2017, 839, 5-14.

13 M. Mora, M. C. Gimeno, R. Visbal, Recent advances in gold–NHC complexes with biological properties. Chem. Soc. Rev. 2019, 48, 447-462.

14 Y. Ching Ong, G. Gasser, Organometallic compounds in drug discovery: Past, present and future, Drug Discovery Today 2020, 37, 117-124.

15 C. Santini, M. Pellei, V. Gandin, M. Porchia, F. Tisato, C. Marzano, Advances in Copper Complexes as Anticancer Agents, Chem. Rev. 2014, 114, 815 – 862.

16 C. Imberti, P. J. Sadler, 150 years of the periodic table: New medicines and diagnostic Agents, Advances in Inorganic Chemistry, 2020, Volume 75, pp. 3-56, Elsevier ed..

17 S. S. Braga, A. M. S. Silva, A New Age for Iron: Antitumoral Ferrocenes, Organometallics 2013, 32, 5626 − 5639.

18 A. Valente, T. S. Morais, R. G. Teixeira, C. P. Matos, A. I. Tomaz, M. H. Garcia, Ruthenium and iron metallodrugs: new inorganic and organometallic complexes as prospective anticancer agents, Synthetic Inorganic Chemistry, chapter 6, 2021, pp. 223-276, Elsevier ed.

19 M. Patra, G. Gasser, The medicinal chemistry of ferrocene and its derivatives. Nat. Chem. Rev. 2017, 1, 10.1038/s41570-017-0066.

20 G. Gasser, I. Ott, N. Metzler-Nolte, Organometallic Anticancer Compounds, J. Med. Chem. 2011, 54, 3-25.

21 S. Daum, V. F. Chekhun, I. N. Todor, N. Yu. Lukianova, Y. V. Shvets, L. Sellner, K. Putzker, J. Lewis, T. Zenz, I. A. M. de Graaf, G. M. M. Groothuis, A. Casini, O. Zozulia, F. Hampel, A. Mokhir, Improved Synthesis of N -Benzylaminoferrocene-Based Platinum Prodrugs and Evaluation of Their Toxicity and Antileukemic Activity. J. Med. Chem. 2015, 58, 2015−2024.

22 A. N. Rodionov, K. Ya. Zherebker, L. V. Snegur, A. A. Korlyukov, D. E. Arhipov, A. S. Peregudov, M. M. Ilyin, M. M. Ilyin Jr., O. M. Nikitin, N. B. Morozova, A. A. Simenel, Synthesis, structure and enantiomeric resolution of ferrocenylalkyl mercaptoazoles. Antitumor activity in vivo. J. Organomet. Chem. 2015, 783, 83-91.

23 L. V. Snegur, A. N. Rodionov, L. A. Ostrovskaya, M. M. Ilyin, A. A. Simenel, Ferrocene-modified imidazoles: One-pot oxalyl chloride-assisted synthesis, HPLC enantiomeric resolution, and in vivo antitumor effects, Appl. Organomet. Chem. 2022, e6681.

24 A. Kondratskyi, K. Kondratska, F. Vanden Abeele, D. Gordienko, C. Dubois, R.-A. Toillon, C. Slomianny, S. Lemière, P. Delcourt, E. Dewailly, R. Skryma, C. Biot, N. Prevarskaya, Ferroquine, the next generation antimalarial drug, has antitumor activity, Sci. Rep. 2017, 7, 15896.

25 G. Jaouen, A. Vessieres, S. Top, Ferrocifen type anti cancer drugs, Chem. Soc. Rev. 2015, 44, 8802-8817.

26 S. Sansook, S. Hassell-Hart, C. Ocasio, J. Spencer, Ferrocenes in medicinal chemistry; a personal perspective. J. Organomet. Chem. 2020, 905, 121017.

27 A. Pilon, A. R. Brás, L. Côrte-Real, F. Avecilla, P. J. Costa, A. Preto, M. H. Garcia, A. Valente, A New Family of Iron(II)-Cyclopentadienyl Compounds Shows Strong Activity against Colorectal and Triple Negative Breast Cancer Cells, Molecules 2020, 25, 1592.

28 G. Agonigi, L. Biancalana, M. G. Lupo, M. Montopoli, N. Ferri, S. Zacchini, F. Binacchi, T. Biver, B. Campanella, G. Pampaloni, V. Zanotti, F. Marchetti, Exploring the Anticancer Potential of Diiron Bis-cyclopentadienyl Complexes with Bridging Hydrocarbyl Ligands: Behavior in Aqueous Media and In Vitro Cytotoxicity. Organometallics 2020, 39, 645-657.

29 V. Ritleng, M. J. Chetcuti, Hydrocarbyl Ligand Transformations on Heterobimetallic Complexes. Chem. Rev. 2007, 107, 797−858.

30 R. Mazzoni, M. Salmi V. Zanotti, C-C Bond Formation in Diiron Complexes, Chem. Eur. J. 2012, 18, 10174-10194.

31 F. Marchetti, F. Constructing Organometallic Architectures from Aminoalkylidyne Diiron Complexes, Eur. J. Inorg. Chem. 2018, 3987–4003.

32 J. Chen, R. Wang, Remarkable reactions of cationic carbyne complexes of manganese, rhenium, and diiron with carbonylmetal anions, Coord. Chem. Rev. 2002, 231, 109-149.

33 G. Agonigi, M. Bortoluzzi, F. Marchetti, G. Pampaloni, S. Zacchini, V, Zanotti, Regioselective Nucleophilic Additions to Diiron Carbonyl Complexes Containing a Bridging Aminocarbyne Ligand: A Synthetic, Crystallographic and DFT Study. Eur. J. Inorg. Chem. 2018, 960–971.

34 G. Ciancaleoni, S. Zacchini, V. Zanotti, F. Marchetti, DFT Mechanistic Insights into the Alkyne Insertion Reaction Affording Diiron μ-Vinyliminium Complexes and New Functionalization Pathways. Organometallics 2018, 37, 3718−3731.

35 L. Biancalana, F. Marchetti, Aminocarbyne ligands in organometallic chemistry. Coord. Chem. Rev. 2021, 449, 214203.

36 L. Biancalana, M. De Franco, G. Ciancaleoni, S. Zacchini, G. Pampaloni, V. Gandin, F. Marchetti, Easily Available, Amphiphilic Diiron Cyclopentadienyl Complexes Exhibit in Vitro Anticancer Activity in 2D and 3D Human Cancer Cells through Redox Modulation Triggered by CO Release. Chem. Eur. J. 2021, 27, 10169–10185.

37 S. Braccini, G. Rizzi, L. Biancalana, A. Pratesi, S. Zacchini, G. Pampaloni, F. Chiellini, F. Marchetti, Anticancer Diiron Vinyliminium Complexes: A Structure–Activity Relationship Study. Pharmaceutics 2021, 13, 1158.

38 H. Ghareeb, N. Metanis, The Thioredoxin System: A Promising Target for Cancer Drug Development, Chem. Eur. J. 2020, 26, 10175 – 10184.

39 M. Bian, R. Fan, S. Zhao, W. Liu, Targeting the Thioredoxin System as a Strategy for Cancer Therapy, J. Med. Chem. 2019, 62, 7309 − 7321.

40 D. Rocco, L. K. Batchelor, G. Agonigi, S. Braccini, F. Chiellini, S. Schoch, T. Biver, T. Funaioli, S. Zacchini, L. Biancalana, M. Ruggeri, G. Pampaloni, P. J. Dyson, F. Marchetti, Anticancer Potential of Diiron Vinyliminium Complexes. Chem. Eur. J. 2019, 25, 14801-14816.

41 S. Schoch, S. Braccini, L. Biancalana, A. Pratesi, T. Funaioli, S. Zacchini, G. Pampaloni, F. Chiellini, F. Marchetti, When ferrocene and diiron organometallics meet: triiron vinyliminium complexes exhibit strong cytotoxicity and cancer cell selectivity. Inorg. Chem. Front., 2022, 9, 5118–5139.

42 G. C. Arya, K. Kaur, V. Jaitak, Isoxazole derivatives as anticancer agent: A review on synthetic strategies, mechanism of action and SAR studies. Eur. J. Med. Chem. 2021, 221, 113511.

43 F. Marchetti, C. Di Nicola, R. Pettinari, C. Pettinari, I. Aiello, M. La Deda, A. Candreva, S. Morelli, L. De Bartolo, A. Crispini, A. Zinc(II) Complexes of Acylpyrazolones Decorated with a Cyclohexyl Group Display Antiproliferative Activity Against Human Breast Cancer Cells. Eur. J. Inorg. Chem. 2020, 1027–1039.

44 V. R. Akhmetova, N. S. Akhmadiev, M. F. Abdullin, L. U. Dzhemileva, V. A. Dyakonov, Synthesis of new N,N-Pd(Pt) complexes based on sulfanyl pyrazoles, and investigation of their in vitro anticancer activity, RSC Adv. 2020, 10, 15116–15123.

45 E. Zanda, N. Busto, L. Biancalana, S. Zacchini, T. Biver, B. Garcia, F. Marchetti, Anticancer and antibacterial potential of robust Ruthenium(II) arene complexes regulated by choice of α-diimine and halide ligands. Chem. Biol. Interact. 2021, 344, 109522.

[46] B. Campanella, S. Braccini, G. Bresciani, M. De Franco, V. Gandin, Federica Chiellini, A. Pratesi, G. Pampaloni, L. Biancalana, F. Marchetti, Metallomics, 2023, mfac096. DOI: 10.1093/mtomcs/mfac096

47 D. Kumar, N. M. Kumar, S. Ghosh, K. Shah, Novel bis(indolyl)hydrazide–hydrazones as potent cytotoxic agents, Bioorg. Med. Chem. Lett. 2012, 22, 212–215.

48 D. K. Kolmel and E. T. Kool, Oximes and Hydrazones in Bioconjugation: Mechanism and Catalysis, Chem. Rev. 2017, 117, 10358 – 10376.

49 P. Krishnamoorthy, P. Sathyadevi, A. H. Cowley, R. R. Butorac, N. Dharmaraj, Evaluation of DNA binding, DNA cleavage, protein binding and in vitro cytotoxic activities of bivalent transition metal hydrazone complexes, Eur. J. Med. Chem. 2011, 46, 3376-3387.

50 S. Rollas, Ş. Güniz Küçükgüzel, Biological Activities of Hydrazone Derivatives, Molecules 2007, 12, 1910-1939.

51 M. C. Rodrıguez-Arguelles, M. Belicchi Ferrari, F. Bisceglie, C. Pelizzi, G. Pelosi, S. Pinelli, M. Sassi, Synthesis, characterization and biological activity of Ni, Cu and Zn complexes of isatin hydrazones, J. Inorg. Biochem. 2004, 98, 313–321.

52 M. Alagesan, P. Sathyadevi, P. Krishnamoorthy, N. S. P. Bhuvanesh, N. Dharmaraj, DMSO containing ruthenium(II) hydrazone complexes: in vitro evaluation of biomolecular interaction and anticancer activity, Dalton Trans., 2014,43, 15829-15840.

53 Q. You Mo, J. Gang Deng, Y. Liu, G. Dong Huang, Z. Wen Li, P. Yu, Y. Gou, F. Yang, Mixed-ligand Cu(II) hydrazone complexes designed to enhance anticancer activity, Eur. J. Med. Chem. 2018, 156, 368-380.

54 G. Bresciani, L. Biancalana, G. Pampaloni, S. Zacchini, G. Ciancaleoni, F. Marchetti, A Comprehensive Analysis of the Metal–Nitrile Bonding in an Organo-Diiron System, Molecules 2021, 26, 7088.

55 T. Y. Luh, Trimethylamine N-Oxide-A Versatile Reagent For Organometallic Chemistry. Coord. Chem. Rev. 1984, 60, 255-276.

56 G. Bresciani, S. Boni, S. Zacchini, G. Pampaloni, M. Bortoluzzi, F. Marchetti, Alkyne – alkenyl coupling at a diruthenium complex, Dalton Trans., 2022, 51, 15703–15715.

57 K. J. Adams, J. J. Barker, S. A. R. Knox, A. G. Orpen, Linking and fragmentation of alkynes at a triruthenium centre, J. Chem. Soc., Dalton Trans., 1996, Pages 975-988.

58 V. G. Albano, L. Busetto, F. Marchetti, M. Monari, S. Zacchini, V. Zanotti, Diiron í-Vinyliminium Complexes from Acetylene Insertion into a Metal - Aminocarbyne Bond, Organometallics 2003, 22, 1326 – 1331.

59 Albano, V. G.; Busetto, L.; Marchetti, F.; Monari, M.; Zacchini, S.; Zanotti, V. Stereochemistry of the insertion of disubstituted alkynes into the metal aminocarbyne bond in diiron complexes. J. Organomet. Chem. 2004, 689, 528–538.

60 L. Busetto, P. M. Maitlis, V. Zanotti, Bridging vinylalkylidene transition metal complexes, Coord. Chem. Rev. 2010, 254, 470–486.

61 G. Bresciani, S. Schoch, L. Biancalana, S. Zacchini, M. Bortoluzzi, G. Pampaloni, F. Marchetti, Cyanide–Alkene Competition in a Diiron Complex and Isolation of a Multisite (Cyano)Alkylidene–Alkene Species, Dalton Trans., 2022, 51, 1936–1945.

62 G. Bresciani, S. Zacchini, G. Pampaloni, F. Marchetti, Carbon − Carbon Bond Coupling of Vinyl Molecules with an Allenyl Ligand at a Diruthenium Complex, Organometallics 2022, 41, 1006 − 1014.

63 C. P. Casey, M. Crocker, G. P. Niccolai, P. J. Fagan, M. S. Konings, Formation of Bridging Acylium and Nitrilium Complexes by Reaction of CO and $CNC(CH_3)_3$ with a Bridging Diiron Methylidyne Complex. J. Am. Chem. Soc. 1988, 110, 6070-6076.

64 L. Busetto, F. Marchetti, S. Zacchini, V. Zanotti, Reactions of Diazo Compounds at í-Vinyliminium Ligands: Synthesis of Novel Dinuclear Azine - Bis(alkylidene) Complexes. Organometallics 2007, 26, 3577 – 3584.

65 A. Notaro, G. Gasser, A. Castonguay, Note of Caution for the Aqueous Behaviour of Metal-based Drug Candidates, ChemMedChem, 2020, 15, 345-348.

66 S. Dasari, P. B. Tchounwou, Cisplatin in cancer therapy: Molecular mechanisms of action. Eur. J. Pharmacol. 2014, 740, 364–378.

67 J. Kalia, R. T. Raines, Hydrolytic Stability of Hydrazones and Oximes, Angew. Chem. Int. Ed. 2008, 47, 7523–7526.

68 R. Vinck, A. Gandioso, P. Burckel, B. Saubaméa, K. Cariou and G. Gasser, Red-Absorbing Ru(II) Polypyridyl Complexes with Biotin Targeting Spontaneously Assemble into Nanoparticles in Biological Media. Inorg. Chem., 2022, 61, 13576-13585.

69 S. Schoch, D. Iacopini, M. Dalla Pozza, S. Di Pietro, I. Degano, G. Gasser, V. Di Bussolo, F. Marchetti, Tethering Carbohydrates to the Vinyliminium Ligand of Antiproliferative Organometallic Diiron Complexes, Organometallics 2022, 41, 514 – 526.

70 G. Agonigi, L. K. Batchelor, E. Ferretti, S. Schoch, M. Bortoluzzi, S. Braccini, F. Chiellini, L. Biancalana, S. Zacchini, G. Pampaloni, B. Sarkar, P. J. Dyson, F. Marchetti, Mono-, Di- and Tetra-iron Complexes with Selenium or Sulphur Functionalized Vinyliminium Ligands: Synthesis, Structural Characterization and Antiproliferative Activity, Molecules 2020, 25, 1656.

71 https://www.agilent.com/cs/library/usermanuals/public/XF_Cell_Mito_Stress_Test_Kit_User_Guide.pdf

72 F. Q. Schafer, G. R. Buettner, Redox environment of the cell as viewed through the redox state of the glutathione disulfide/glutathione couple, Free Rad. Biol. Med. 2011, 30, 1191-1212.

73 Q. Du, L. Guo, M. Tian, X. Ge, Y. Yang, X. Jian, Z. Xu, Z. Tian, Z. Liu, Potent Half-Sandwich Iridium(III) and Ruthenium(II) Anticancer Complexes Containing a P^O-Chelated Ligand, Organometallics 2018, 37, 2880-2889.

74 Menges, F. "Spectragryph - optical spectroscopy software", Version 1.2.5, @ 2016-2017, http://www.effemm2.de/spectragryph.

75 Fulmer, G. R.; Miller, A. J. M.; Sherden, N. H.; Gottlieb, H. E.; Nudelman, A.; Stoltz, B. M.; Bercaw, J. E.; Goldberg, K. I. NMR Chemical Shifts of Trace Impurities: Common Laboratory Solvents, Organics, and Gases in Deuterated Solvents Relevant to the Organometallic Chemist. Organometallics 2010, 29, 2176–2179.

76 Willker, W.; Leibfritz, D.; Kerssebaum, R.; Bermel, W. Gradient selection in inverse heteronuclear correlation spectroscopy. Magn. Reson. Chem. 1993, 31, 287-292.

77 Albano, V. G.; Busetto, L.; Monari, M.; Zanotti, V. Reactions of acetonitrile di-iron μ-aminocarbyne complexes; synthesis and structure of [Fe2(μ-CNMe2)(μ-H)(CO)2(Cp)2]. J. Organomet. Chem. 2000, 606, 163–168.

78 Sheldrick, G. M. Crystal structure refinement with SHELXL. Acta Crystallogr. C2015, 71, 3-8.

79 When the brown precipitate formed from diiron vinyliminium complexes in aqueous media was isolated, this was analyzed by IR and RAMAN spectroscopy, revealing the prevalence of iron oxides in admixture with minor amounts of the starting complex. See references [28] and [40].

80 Rundlöf, T.; Mathiasson, M.; Bekiroglu, S.; Hakkarainen, B.; Bowden, T.; Arvidsson, T. Survey and qualification of internal standards for quantification by ^{1}H NMR spectroscopy. J. Pharm. Biomed. Anal. 2010, 52, 645-651.

81 Rice, N. M.; Irving, H. M. N. H.; Leonard, M. A. Nomenclature for liquid-liquid distribution (solvent extraction) (IUPAC Recommendations 1993). Pure & Appl. Chem. 1993, 65, 2373-2396.

82 Biancalana, L.; Batchelor, L. K.; Funaioli, T.; Zacchini, S.; Bortoluzzi, M.; Pampaloni, G.; Dyson, P. J.; Marchetti, F. α-Diimines as Versatile, Derivatizable Ligands in Ruthenium(II) p-Cymene Anticancer Complexes. Inorg. Chem. 2018, 57, 6669-6685.